



12-2002

Biomechanical behaviors of the human triceps surae during landing activities

Kurt Gavin Clowers
University of Tennessee

Follow this and additional works at: https://trace.tennessee.edu/utk_gradthes

Recommended Citation

Clowers, Kurt Gavin, "Biomechanical behaviors of the human triceps surae during landing activities. " Master's Thesis, University of Tennessee, 2002.
https://trace.tennessee.edu/utk_gradthes/5900

This Thesis is brought to you for free and open access by the Graduate School at TRACE: Tennessee Research and Creative Exchange. It has been accepted for inclusion in Masters Theses by an authorized administrator of TRACE: Tennessee Research and Creative Exchange. For more information, please contact trace@utk.edu.

To the Graduate Council:

I am submitting herewith a thesis written by Kurt Gavin Clowers entitled "Biomechanical behaviors of the human triceps surae during landing activities." I have examined the final electronic copy of this thesis for form and content and recommend that it be accepted in partial fulfillment of the requirements for the degree of Master of Science, with a major in Human Performance and Sport Studies.

Songning Zhang, Major Professor

We have read this thesis and recommend its acceptance:

David R. Bassett, Wendell P. Liemohn

Accepted for the Council:

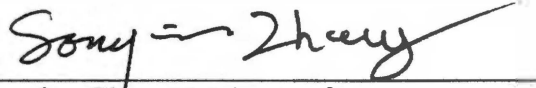
Carolyn R. Hodges

Vice Provost and Dean of the Graduate School

(Original signatures are on file with official student records.)

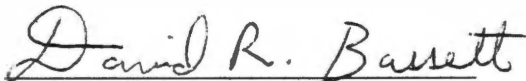
To the Graduate Council:

I am submitting herewith a thesis written by Kurt Gavin Clowers entitled "Biomechanical Behaviors of the Human Triceps Surae During Landing Activities." I have examined the final paper copy of this thesis for form and content and recommend that it be accepted in partial fulfillment of the requirements of the degree of Master of Science, with a major in Human Performance and Sport Studies



Songning Zhang, Major Professor

We have read this thesis
and recommend its acceptance:

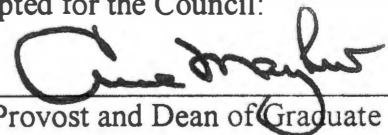


David R. Bassett, Ph.D.



Wendell P. Liemohn, Ph.D.

Accepted for the Council:



Vice Provost and Dean of Graduate Studies

**Biomechanical Behaviors of the Human Triceps Surae
During Landing Activities**

**A Thesis
Presented for the
Master of Science Degree**

The University of Tennessee, Knoxville

**Kurt Gavin Clowers
December 2002**

DEDICATION

Thesis
2002
.C55

This thesis is dedicated to my father, Grant Clowers, whose major objective in life was to provide the very best for his family. He died while successfully achieving his goal.

ACKNOWLEDGEMENTS

I would like to thank my mother, Ingrid Clowers, who supported me through the death of my father. She has truly lived up to the calling of mother, always abounding with encouragement and championing my father's dreams for his children. She sacrificed more than could have even been expected of any mother.

I would also like to express gratitude for my wife Cheryl. She provided the wind beneath my wings so that I could soar and accomplish this task. She sacrificed much so I could pursue my education and accomplish my goals.

Next I would like to thank my major advisor, Dr. Songning Zhang. He provided guidance and instruction whenever asked, he supplied me with an education that cannot come from any text or lecture, and he taught me the fundamentals of research and perseverance.

Also, I would like to thank my committee members Dr. Wendell Liemohn and Dr. David Bassett. They provided assistance and were very patient with me in completing this project.

Lastly, I would like to express my appreciation to Dr. Ton van den Bogert and Dr. Arthur J. van Soest who provided who provided technical advice for this project.

ABSTRACT

The purpose of this study was to investigate biomechanical behaviors of human triceps surae in landing activities using a Hill-type muscle model. Ten healthy male subjects (23 ± 3 yrs) performed five trials of drop landing from a height of 60 cm in each of four conditions: a normal landing (NL); a stiff landing that required the subject to perform a NL but with minimal knee flexion (SL); a SL but landing flat footed (SF); and a stiff landing while landing on the toes only (SC). Sagittal kinematic (120 Hz), ground reaction forces (GRF) and moments (1200 Hz) were recorded simultaneously. Using an inverse dynamics approach, ankle moment and triceps surae muscle forces were computed. In addition, the triceps surae muscle force and ankle moment were estimated using the Hill-type model. A one-way analysis of variance (ANOVA) was used to evaluate selected variables with the significant level set at $P < 0.05$. The mean peak GRF values for NL, SL, SF and SC were 38.0, 49.2, 35.5 and 58.6 N/kg, respectively. The mean VGRF of peak associated was found to be significantly different between each condition except NL and SC. The Hill model predicted the peak triceps surae forces at 54.6, 65.0, 40.7, and 62.1 N/kg for NL, SL, SF, and SC respectively. The mean peak plantar flexing moments for NL, SL, SF, and SC were 2.2, 4.0, 2.8, and 4.4 Nm/kg respectively while the estimated plantar flexing moment had values of 3.7, 4.6, 4.7 and 3.2 Nm/Kg for the same conditions. Greater discrepancy was observed between the experimental and estimated joint moment and muscle force for SF. The Hill model was considered to be a good predictor of the eccentric muscle force in the landing activity for NL, SL, and SC except for SF.

TABLE OF CONTENTS

CHAPTER	PAGE
I. INTRODUCTION.....	1
Problem Statement.....	5
Hypotheses.....	6
Delimitations.....	6
Limitations.....	7
Assumptions.....	8
II. LITERATURE REVIEW.....	9
Modeling.....	9
Landing.....	18
Muscle Geometry.....	20
Additional Models.....	25
The Distribution Moment Model.....	25
Other Models.....	26
III. RESEARCH METHODS.....	29
Experimental Methods.....	29
Subjects.....	29
Instrumentation.....	29
Kinematics.....	30
Force Platform.....	30
Electrogoniometer.....	31
Synchronization.....	32
Experimental Protocol.....	32
Data Processing.....	34
Calculation of Center of Gravity (COG).....	35
Joint Kinetics and Muscle Model.....	36
IV. BIOMECHANICAL BEHAVIORS OF THE HUMAN TRICEPS SURAE DURING LANDING ACTIVITIES.....	40
Introduction.....	40
Methods.....	43
Subjects and Experimental Protocol.....	43
Instrumentation.....	44
Joint Kinetics and Muscle Model.....	45
Results.....	46
Discussion.....	54
LIST OF REFERENCES.....	63

APPENDICES	67
Appendix A	68
Appendix B	70
Appendix C	72
Appendix D	74
Appendix E	76
Appendix F	78
Appendix G	80
Appendix H	82
Appendix I	84
Appendix J	86
Appendix K	88
Appendix L	90
Appendix M	92
Appendix N	94
Appendix O	96
Appendix P	98
Appendix Q	100
Appendix R	102
Appendix S	106
Appendix T	110
 VITA.....	 115

LIST OF TABLES

TABLE	PAGE
1. Coefficients for predicting change in muscle length as described by Grieve et al	73
2. Anthropometric measurements and definitions.....	75
3. Subject Information	81
4. Means and standard deviations of angular kinematic variables for the three joints of the lower extremity	47
5. Condition means and standard deviations of VGRF	49
6. Condition means and standard deviations of VGRF	83
7. Condition means and standard deviations of angular kinematic hip joint variables..	97
8. Condition means and standard deviations of angular kinematic knee joint variables	99
9. Subject means and standard deviations of angular kinematic hip joint variables....	103
10. Subject means and standard deviations of angular kinematic knee joint variables	107
11. Subject means and standard deviations of angular kinematic ankle joint variables	111

LIST OF FIGURES

FIGURE	PAGE
1. A model of the triceps surae muscle tendon complex as adopted from Bobbert et al.	11
2. Positions of reflective markers at shoulder (S), hip (H), knee (K), ankle (A), heel (H), and fifth metatarsal (M).....	31
3. Drop Setup.....	34
4. Free body diagram of the foot, and equations for calculation of dorsi-flexing moment.....	37
5. Representative curves for hip joint angle for (a) normal landing (NL), (b) stiff lading with minimal knee flexion (SL), (c) stiff landing but landing flat footed (SF), and (d) stiff landing but landing only on the toes and contracting the calf muscle (SC)	85
6. Representative curves for knee angle joint for (a) normal landing (NL), (b) stiff lading with minimal knee flexion (SL), (c) stiff landing but landing flat footed (SF), and (d) stiff landing but landing only on the toes and contracting the calf muscle (SC)	87
7. Representative curves for ankle joint angle for (a) normal landing (NL), (b) stiff lading with minimal knee flexion (SL), (c) stiff landing but landing flat footed (SF), and (d) stiff landing but landing only on the toes and contracting the calf muscle (SC)	89
8. Representative curves for hip joint angular velocity for (a) normal landing (NL), (b) stiff lading with minimal knee flexion (SL), (c) stiff landing but landing flat footed (SF), and (d) stiff landing but landing only on the toes and contracting the calf muscle (SC)	91
9. Representative curve for knee joint angular velocity for (a) normal landing (NL), (b) stiff lading with minimal knee flexion (SL), (c) stiff landing but landing flat footed (SF), and (d) stiff landing but landing only on the toes and contracting the calf muscle (SC)	93
10. Representative curves for ankle joint angular velocity for (a) normal landing (NL), (b) stiff lading with minimal knee flexion (SL), (c) stiff landing but landing flat footed (SF), and (d) stiff landing but landing only on the toes and contracting the calf muscle (SC)	95

11. Representative GRF curves for (a) normal landing (NL), (b) stiff landing with minimal knee flexion (SL), (c) stiff landing but landing flat footed (SF), and (d) stiff landing but landing only on the toes and contracting the calf muscle (SC)	49
12. Representative ensemble curves of estimated and experimental triceps surae forces from one subject for (a) normal landing (NL), (b) stiff landing with minimal knee flexion (SL), (c) stiff landing but landing flat footed (SF), and (d) stiff landing but landing only on the toes and contracting the calf muscle (SC)	50
13. Representative ensemble curves of estimated and experimental triceps surae moments from one subject for (a) normal landing (NL), (b) stiff landing with minimal knee flexion (SL), (c) stiff landing but landing flat footed (SF), and (d) stiff landing but landing only on the toes and contracting the calf muscle (SC)	52
14. Representative curves from a single subject that depicts examples of (a) overestimated force output (b) average force output (c) underestimated force output calculated by the Hill model for SC	58

Chapter I

Introduction

Eccentric muscle actions play a vital role in daily living activities. They occur in common tasks such as lowering a pencil to a desktop or the quadriceps muscle lengthening as a person sits down in a chair. In many sport activities, eccentric muscle contractions are a crucial part of the landing phase. In a landing activity, the gastrocnemius and soleus muscles are shown to be an part of the impact absorption process [2, 3, 5].

In a typical concentric contraction a skeletal muscle develops tension as the shortening velocity increases. However, if a resistance applied to the muscle becomes too great to resist, it lengthens but only after producing more tension. This is known as an eccentric muscle contraction. At the sarcomere level, the active force generated by a single cross-bridge occurs because actin filaments at each end of the sarcomere slide inward on myosin filaments pulling the Z-lines toward the center of the sarcomere and thus shortening it and the whole muscle. The rate of shortening of a sarcomere depends on the ability of many myosins to move to their next respective actin along thin filaments. The force of resistance, which tends to lengthen the sarcomere, contrasts this process and for each cross bridge cycle energy is consumed. The formation of cross-bridges and sarcomere shortening results in potential energy that is transformed into mechanical events of muscle tension and shortening. However, if immediately after the binding reaction occurs and the cross-bridge is forcibly pulled backward, the actin-myosin bond

breaks before the transfer of energy can occur. Such is the case in an eccentric muscle contraction [36]. Thus it becomes clear from this forced muscle lengthening that the muscle itself becomes more susceptible to injury.

It is a common belief that muscle strain injury occurs in response to forcibly stretching the muscle [13]. Garret reported that muscle strain injuries occur most often during eccentric muscle contractions and that biarticular muscles are more at risk for such an injury [13]. Many studies have documented the fact that injury may occur in a muscle after eccentric exercises. Friden et al. [12] demonstrated a total disruption in the myofibrillar Z-bands after as many as six days following bouts of eccentric exercise. Similarly, Newham et al. [27] reported that as many as six weeks after performing eccentric exercises, the plasma creatine kinase (CK) values of the participating subjects, an indicator of muscle damage, were elevated. In a study by Brown et al. [8], they observed not only does eccentric exercise cause skeletal muscle tissue damage but also connective tissue damage. A more recent study by Takekura et al. [37] showed downhill running exercises resulted in dramatic changes in the excitation-contraction coupling process in skeletal muscle fibers as well as elevated plasma CK values.

Furthermore, additional studies have shown that strength training with an accentuated eccentric component or eccentric only training provides no gain in concentric strength and limits the amount of concentric peak torques that can be produced [14, 22]. Leger et al. [24] demonstrated that eccentric exercise decreases maximal voluntary contractions (MVC) and causes motor impairment. In another study Leger et al. [25] showed that eccentric exercise reduces the amount of torque a muscle can produce and cause joint stiffness.

One solution to this problem is that muscle models can be used to study the contractile behaviors of muscles in an effort to better understand injury mechanisms. A muscle model is an attempt to represent reality [18]. Better still it is a mathematical description used to describe the behavior of muscles' contractile conditions. The contractile property of muscles undergoing concentric contractions is better understood and well documented; however, for muscles undergoing eccentric contractions this is not the case.

When using a model to describe the behavior of muscles for certain contractile conditions, certain biological considerations must be kept in mind. The first such consideration is that the geometry of the muscle must be realized. The geometry of the muscle is used for the derivation of equations that describe the contractile behavior. If the arrangement of the muscle fibers is assumed to be bound by straight lines then analytical expressions can be developed to describe the muscle action. If the muscle is assumed to be pennate where the long axis of the muscle fiber is at an oblique angle with respect to the axis of shortening, then the model becomes more mathematically complex [11]. Also, muscle model schematics must be understood before investigating muscle contractile behaviors. The schematics of a muscle model are typically represented by the findings of A. V. Hill. In a classic study, Hill [21] concluded that skeletal muscle is composed primarily of a contractile element (CE) and an elastic element in series (SE) with CE. The active force produced by a muscle is generated in CE and displays three properties: the length-tension property where the tension generated by the muscle is a function of the muscle physiological cross sectional area (PSCA); the force-velocity property where the muscle force is a function of the rate of change in muscle length; and

the power-velocity property where the muscle power generated is a function of the muscle's rate of change in length [11].

In essence, there are three types of muscle models employed to study the biomechanical behavior of muscles. One type of model is called the Huxley type or biophysical cross-bridge model. This model was first proposed by Andrew Fielding Huxley in 1957 and is based on the binding and unbinding of actin and myosin myofilaments [43]. The advantages to using this type of model are that it is a concise mathematical description of the way muscles are believed to work and important relations between mechanics, energetics, and chemical kinetics in muscle can be studied using this model. The disadvantage in choosing this type of model for study is that it is extremely complex from the viewpoint of musculo-skeletal mechanics [10].

The second type of model used to investigate the contractile behavior of muscles is the Distribution Moment Model (DM). Zahalak [42] derived the DM model from Huxley model. It is a bridge between the Huxley type model and the Hill model; however, it relies heavily on actin myosin bonding and unbonding [42]. Advantages in using this type of model include that it is a structural model based on the assumed interaction of thin (actin) and thick (myosin) myofilaments via cross-bridges, and the corresponding force production, while remaining mathematically tractable [10, 43]. On the other hand, the drawback to using the DM model is its mathematical complexity when compared to the Hill model, and it is typically used in biophysical research for the quantification of heat production and energetics.

The last type of muscle model used to study the contractile behavior of muscles is the Hill model. The Hill model is named after Archibald Vivian Hill and is based on his

famous experiment on the heat production during skeletal muscle shortening [21]. In that study he deduced the force-velocity relationship of muscles using part of an equation for a rectangular hyperbola. The benefits of using the Hill model consisting of CE and SE element is that the properties of a tendon can readily be determined; therefore, deriving the constitutive properties of SE becomes much easier. Also the Hill model is associated with qualitatively correct predictions for a variety of contractile conditions [10].

Engineers and biologists also universally accept the Hill model as an appropriate representation of muscle mechanics [43]. The major weakness of the Hill model is that recent literature has shown that the aponeurosis of a muscle contributes to SE and that the latter has been shown to lie in the cross-bridge, the contractile portion of the Hill model [10]. Also, the Hill equation must be modified in order to predict certain contractile conditions because the original equation is valid for restricted contractile conditions such as maximal activation and shortening contraction at or near optimal length [10, 40].

Problem Statement

Muscle models have been used extensively to simulate and investigate numerous types of human movement. Spoor [34] used a muscle model of the finger to determine that without intrinsic muscles internal stabilization of the finger is impossible and only dorsodistal directed forces on the fingertip can be balanced. Nussbaum et al. [28] used a muscle model to examine predicted muscle and spinal forces to assumed muscle lines-of-action. However, a large body of the literature on muscle modeling includes topics on jumping [1, 4, 6, 29, 31-33]. Typically, these research studies examine the role of concentrically contracting muscles or simulate muscles only undergoing concentric

contractions. Very limited research is provided on muscles undergoing eccentric muscle contractions [9]. Also, the research does not concentrate on just one component of the contractile element [19]. Instead, the literature is more encompassing of the contractile element, series elastic element, and parallel element [29, 31-33, 40, 42, 44]. Therefore, the purpose of this study is to investigate the biomechanical behaviors of the human triceps surae in landing activities using a Hill type model.

The results of this study may provide a better understanding of the injury mechanisms that occur during eccentric muscle contractions, performance enhancement and prevention of sport injuries, expressly during landing activities.

Hypotheses

The following hypotheses were tested:

- 1) The muscle force generated by the gastrocnemius and soleus is significantly higher for the stiff-legged toe-only landing technique than the other stiff-legged and toe-heel landings.
- 2) The moment about the ankle is greater for stiff-legged landing techniques than toe-heel landings.

Delimitations

The study was conducted within the following delimitations:

- 1) Ten active and healthy male subjects were selected from the student population at The University of Tennessee. They had no impairments of the lower extremities.

- 2) Each subject performed four test conditions, which included drop landings from an overhead drop bar set at 60 cm that was measured from the calcaneus to the landing surface.
- 3) Biomechanical signals were collected and analyzed for duration from 20 ms prior to contact and 100 ms after contact.
- 4) Data were collected at 1200 Hz from a force platform (OR6-7, AMTI), one electrogoniometer (Penny+Giles Biometrics Ltd), and at 120 Hz from a video camera (JVC, GR-DVL 9800) for each trial of the landing activity.

Limitations

The study was limited by the following factors:

- 1) Subjects were limited to the student population at The University of Tennessee.
- 2) Possible errors from placement and digitizing of the reflective markers. Other errors such as perspective error and marker placement are acknowledged. Minimization of these errors is accomplished by understanding accurate anatomical information and repeated practice of marker placement. Furthermore, the use of an automatic digitizing program, such as Ariel Performance Analysis System (APAS), helped limit possible errors caused by the digitization of reflective markers.
- 3) Inherent errors in this study came from the force platform, accelerometer, and/or digital video systems. Errors of force platform and high-speed video systems are always present but were considered acceptable within the specifications of the manufacturers. Confining the activity to the sagittal plane controlled errors caused by out of plane motion.

4) The potential errors in this study are due to the difference in sampling frequency of the force platform (1200Hz) and the digital video system (120Hz), and synchronization of the systems. Synchronization accuracy between the force and video systems was limited by the sampling rate of the slower system. The video system has a sampling error of ± 0.08 frames/second, resulting a maximum error of only 0.67 ms.

Assumptions

The following assumptions were made for this study:

- 1) Drop landings could be modeled mechanically.
- 2) Biomechanical measurements used were sufficient for analyzing effects of drop landings with different landing techniques.
- 3) Biomechanical instruments used were accurate.
- 4) All subjects were free of injuries to the lower extremity at the time of testing.
- 5) The performance of the subjects was symmetrical, so only the right side was assessed for the kinematics and GRF.
- 6) For the Hill model, the contractile element is in series with the series elastic element.

Chapter II

Literature Review

The purpose of this study was to investigate the biomechanical behaviors of the human triceps surae in landing activities. Therefore, the objective of this literature review is to present research findings concerning muscle modeling and more specifically muscle models of the triceps surae muscle tendon complex. Further research is reviewed on landing, muscle geometry, and other relevant studies related to muscle modeling.

Modeling

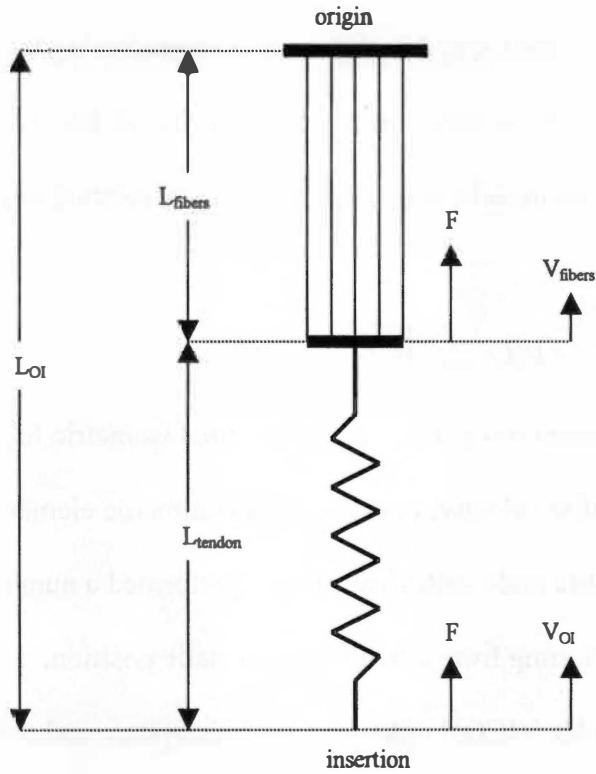
Bobbert et al. [4] conducted a study to gain further understanding of how the human triceps surae muscle-tendon complex behaves during plantar flexion in jumping. Ten trained male subjects performed a number of one-legged vertical countermovement jumps with their non-preferred leg. Ground reaction forces were recorded using a force platform (Kistler type 9281 B) sampled at 500 Hz. The coordinates and positions of six anatomical landmarks were determined using a motion analyzer (Dynamic Frame). The authors constructed a model of the human triceps surae muscle-tendon complex to test their hypothesis under the following assumptions:

- All muscle fibers have the same length and obey the same force-length and force-velocity relationships
- Effects of line of pull between muscle fibers and line of pull of muscle are neglected
- Tissue of aponeuroses has same elastic behavior as tissue of tendons

- Muscle fiber is in series with tendon fiber whose length is obtained by subtracting muscle fiber length from distance between origin and insertion
- Each tendon fiber has a cross sectional area of AN^{-1} , A= cross sectional area of insertion
- Series elastic component is negligible
- Force-velocity relationship is based on Hill equation

From these assumptions the model can be schematized as shown in Figure 1, which is a modified Hill model (see Appendix A for derivation). They used the velocity with which the origin approaches the insertion (V_{OI}) of the muscle as an input to their model. The results of this study indicated that the shortening velocity of the muscle fibers (V_{fibers}) have higher values for the soleus than for the gastrocnemius both in the experimental results and the model. In the beginning of the push-off phase the experimental plantar flexion moment actually increased while the calculated plantar flexion moment from the model decreased. Also, during the last part of the takeoff phase the shortening velocity of the origin and insertion (V_{OI}) rapidly increased while the model found a decline in the plantar flexing moment.

When performing a maximal vertical jump, it is surprising to learn that the initial starting position of the jump does not affect execution. To understand this phenomenon Soest et al. [32] investigated whether or not the successful performance of squat jumps initiated from various starting positions was achieved by using a single selected muscle stimulation pattern. To test their hypothesis, they used a muscle model and a simulation



Where:

- L_{OI} distance between origin and insertion
- L_{fibers} length of muscle fibers
- L_{tendon} length of tendon
- V_{OI} velocity with which origin approaches zero
- V_{fibers} shortening velocity of muscle fibers
- F exerted force

Figure 1. A model of the triceps surae muscle tendon complex as adopted from Bobbet et al. [4]

approach. The muscle model was composed of six muscle groups (gluteal muscle, hamstrings, vasti, rectus femoris, soleus, and gastrocnemius) representing the major muscle groups that contribute to extension of the lower extremity. A Hill-type muscle model was used to represent these muscles and the force-velocity relation was based on Hill's classical equation:

$$\left[\frac{F_{CE} + a}{F_{MAX}} \right] \cdot \left[\frac{V_{CE} + b}{L_{CE(OPT)}} \right] = c$$

where F_{CE} is the contractile element force, F_{MAX} is the maximal isometric force, V_{CE} is the contractile element contraction velocity, $L_{CE(OPT)}$ is the contractile element optimal length, and c is constant. Six elite male volleyball players performed a number of maximum height squat jumps starting from a freely chosen static position. Kinematic data were gathered using a 100-Hz VICON video and analysis system and the ground reaction forces were gathered using a force platform (Kistler 9281 B). Upon comparison of experimental data to simulation data, the kinematics patterns were similar in that a continuous extension occurs at all joints except at the ankle joint. The jump height for the model is 13% lower than that observed experimentally and the mechanical work done by the muscles during takeoff was higher in the simulation. They concluded that a single control pattern that works for a wide range of starting positions could be found.

Soest et al. [31] investigated to what extent the spring-like behavior resulting from the force-length relationship and the stabilizing effect of the force-velocity characteristic of muscle contributed to the successful open-loop control of an inverted pendulum like musculoskeletal system. The authors used modeling and a simulation approach to investigate their hypothesis by examining a maximum-height squat jump. The authors examined the role of muscle dynamics in reducing the effect of perturbations

applied to the musculoskeletal system; a direct simulation approach was used in which the movement of the skeletal system is calculated from independent control signals. They compared two kinds of open loop control signals: $STIM(t)$ representing the neural input to the muscles where the dynamics are included and $MOM(t)$ representing the net joint moment where the dynamics is excluded. They performed three types of simulations. The first simulation applied the MOM control to the reference initial state, where the movement is identical to the movement pattern of applying STIM control. Next perturbations were applied to the system under MOM control and the subsequent movement is seriously affected. Last, the effect of the muscle dynamics on the system sensitivity to perturbations is investigated. The skeletal model consisted of four rigid segments: foot, lower legs, upper legs, and head-arms-trunk (HAT). The skeletal model was described by four second-order differential equations generated by a software package (SPACAR). The dynamic equations express the acceleration of the skeletal system as a function of position, velocity, and active forces. The muscle model included the gluteal muscles, hamstrings, vasti, rectus femoris, soleus, and gastrocnemius. A Hill type model was used to represent the muscles in which STIM served as input of the model and the moment exerted on the skeleton at the joints served as output. They found that when applying MOM control, the movement is dramatically affected with the jump height reduced by 0.09 m. When the authors applied both MOM and STIM to their model they found that the muscle dynamics reduces the effect of perturbations significantly.

Bobbert et al. [1] examined the role of time available for force development and the reutilization of stored elastic energy in enhancing the countermovement jump (CMJ)

performance over squat jump (SJ) performance. The kinematics, kinetics, and muscle electrical activity of six male volleyball players were monitored during maximum CMJ and SJ. The kinematics and electromyographic activity were also used as input to a model of the musculoskeletal system that calculated internal states and roles of individual muscle-tendon complexes. The model displayed the effects of the stimulation histories in CMJ and SJ on joint moments and joint work. The kinematics were collected using four high-speed cameras (VICON, 200 HZ) and the ground reaction forces were gathered using a force platform (Kistler 9281 B). The results revealed that CMJ height is greater than SJ height, in part, due to the fact that the countermovement allowed the subjects to attain greater joint moments. Thus, the greater height was achieved in CMJ because more work could be produced immediately following the countermovement during the jump, which allowed the extensor muscles to build up force prior to shortening.

Cole et al. [9] compared the force-time response of maximally activated muscle during iso-velocity stretches at different velocities using the Hill Model and the Distribution Moment Model (DM). The Hill model and the DM model were used to simulate force production during stretch of the cat soleus muscle. They performed the stretch of the cat soleus muscle at a constant velocity with an amplitude of 4 mm. The stretch velocities used were set at 7.2 and 400 mm s⁻¹. FORTRAN was linked to a DADS multibody dynamics software so that differential equations could be solved for each state equation for each muscle model. The single state equation for the Hill model was

$$\dot{L}_{CE} = f[L_{CE}(t), L_{MT}(t)],$$

where L_{CE} was the length of the contractile element, and L_{MT} was the length of the muscle tendon unit. The state equation for the DM model was

$$Q(t) = f[Q(t), \dot{L}_{MT}(t)],$$

and formulated in terms of three, nonlinear, simultaneous differential equations for the velocities of the state variables $Q = \{Q_0, Q_1, Q_2\}$. Upon comparison to the experimental data, the Hill model provided a good prediction of the kinetic response to slow and fast stretch of maximally stimulated muscle. More specifically, the non-optimized Hill model underestimated the force over the duration. However the force predicted during stretch using the optimized Hill model was similar to the experimental results. The DM model predicted forces at slow stretch well but failed at higher velocities.

A model was designed to test the hypothesis that the biarticularity of the gastrocnemius contributes significantly to vertical jumping achievement by Soest et al. [33]. In general, the authors determined how high the model could jump with intact gastrocnemius (GAS) when the push-off is started from a static squatting position. Then the GAS was changed to a monoarticular plantarflexor, and the maximum height was determined. The difference between these two jump heights is an indicator of the GAS biarticularity contribution to jump height. More specifically, a skeletal model consisting of the foot, leg, thigh, and trunk was developed. The skeletal model was developed in SPACAR, a software system for simulation of the kinematics and dynamics of multibody mechanical systems. The muscles modeled in this study were the glutei, hamstrings, vasti, rectus femoris, soleus, and gastrocnemius. A Hill-type muscle model consisting of a contractile element, a series elastic element, and an elastic element parallel to the contractile was used to represent the respective muscles. The input for the muscle model was the level of STIM. In the experimental portion of this study six male volleyball players performed a number of jumps starting from a squatting position with no

countermovement. The experimental data and the simulation proximodistal sequence in muscle activation were found to be similar. Furthermore, simulation results concerning the optimal jump were compared with the experimental data and were found to be similar. The joint angle versus the joint moment for the hip, knee, and ankle joints for the experimental group and simulation group corresponded to one another. However, there was a difference in jump height between the two groups. The jump height for the simulation group was less than the experimental group because the position of the center of mass at the instant of take off was less for the simulation group. The contribution of the biarticularity versus monoarticularity for the GAS was minimal. Results indicated that the GAS forces are lower in the monoarticular GAS and the jump height was only 10 mm less than for the biarticular GAS. The authors concluded that the way in which the moment arm at the knee of the GAS depends on knee angle decides the effect of the biarticularity of the GAS has jump height.

Bobbert et al. [6] investigated the effects of systematic manipulations of both control and muscle strength on vertical jump height using a model of the human musculoskeletal system. The objective of this study was to provide a theoretical framework that will benefit coaches and athletes involved in jump training programs. Six male volleyball players performed a number of squat jumps with no countermovement. Kinematic data of the 5th metatarsophalangeal joint, lateral malleolus, lateral epicondyle of femur, major trochanter, and trunk were all recorded (VICON) at 100 Hz. The ground reaction forces were also recorded (Kistler, 9281B) and electromyograms of the semitendinous, biceps femoris, gluteus maximus, rectus femoris, vastus medialis, gastrocnemius, and soleus were taken. The jump height was defined as the difference

between the height of the center of mass (COM) at the apex of the jump and the height of the COM when the subject was standing on the ground. This method was used to obtain the jump height for the simulation. The authors used a forward dynamic model of the musculoskeletal system to simulate the vertical jumps. The input for this model was STIM of six muscles of the lower extremity as a function of time and the movements of body segments were used as output for this model. A Hill-type muscle was used to represent six muscle groups including the hamstrings, gluteal muscles, rectus femoris, vasti, gastrocnemius, and soleus. The Hill model was the same as described by Soest et al. [31]. The model is described by a set of 20 coupled nonlinear first-ordinary differential equations. The input for this model was the active state related to muscle stimulation, STIM. However, the jump height of the model was 0.05 m less than the experimental model because the head, arms, and trunk segment of the skeletal model was rigid whereas the subjects are able to do work by extending their trunks. Also, this study was designed to investigate the effects of systematic manipulations of both control and muscle strength on vertical jump height. Their results indicated that muscle strength determines the maximal jump height that can be reached; actual performance relies crucially on the tuning of muscle control properties.

One major function of biomechanical research is to better understand how intermuscular control, inertial interactions among body segments, and musculotendon dynamics coordinate a complex human motion. Pandy et al. [29] constructed an optimal control model for studying maximum height jumping. The model allowed them to simultaneously synthesize the time histories of segmental motions, muscle forces, muscle activations, and incoming neural controls. The human body was depicted as a four-

segment model with planar articulated linkage and frictionless joints. Eight lower extremity musculotendon units provided the actuation including the soleus, gastrocnemius, other plantarflexors, tibialis anterior, vasti, recutis femoris, hamstrings, and gluteus maximus. The authors used Newton's laws to derive the dynamical equations of motion for the four-segment model. The equations for body segment dynamics, excitation-contraction dynamics, and equations for the overall musculotendinoskeletal system can be found in Appendix H. The mechanical behavior of the muscle was described by a Hill type equation. The muscle model consisted of a contractile element, which modeled the force-length-velocity characteristics. It also contained a series elastic element that modeled short-range stiffness and a parallel elastic element that modeled passive properties. A first-order differential equation depicting the relationship between the time rate of change of tendon force and musculotendon length and velocity (l^{MT} , and v^{MT}), muscle activation $a(t)$, and tendon force (P^T):

$$\frac{dP^T}{dt} = f\left[P^T, l^{MT}, v^{MT}, a(t)\right]; \quad 0 < a(t) \leq 1$$

The published experimental results of a maximum squat jump were similar to the results predicted by their model. The optimal control solution of their model showed a proximal-distal pattern of muscle activation. They also found that the optimal performance for maximum jump height is achieved when the muscle activation pattern is sequenced in the order of the hip, knee, and ankle, which is in agreement with the literature.

Landing

Self et al. [30] examined maximum vertical GRF and maximum tibial acceleration, and ankle kinetics in four different landing activities. The four landing strategies included a natural landing with bent knees (BN), stiff knees (SN), knees stiff while absorbing force through plantar flexors (SP), and stiff knees while landing on the heels (SH). The Achilles tendon force acting on the foot during each landing type was calculated using inverse dynamics. BN drops showed greater knee flexion than all other drops while SH showed the greatest forces and were significantly higher than all other landing strategies. The maximum Achilles tendon force was highest for SP while the SH generated the lowest forces. The Achilles force values obtained proved to have a linear relationship with gastrocnemius length in that the force increased linearly with length.

Zhang et al. [45] investigated changes in energy absorption of lower extremity joints for different landing heights and techniques. They recruited nine physically active subjects. The experiment was divided into two test sessions. The first session was designed to allow the subjects to gain a familiarity with the protocol and to obtain a range of maximum knee flexion. In the next session the right sagittal view of the subject was recorded by high-speed video cameras (200 Hz, Motion Analysis Corporation) and GRF were recorded by two force platforms (1000 Hz, AMTI). The subjects were asked to land from heights of 0.32 m, 0.62 m, and 1.03 m with three landing techniques: soft landing (SFL), normal landing (NML), and stiff landing (STL). The ground reaction forces recorded demonstrated the typical time-history curves of two distinctive maximums with first peak (F1) related to toe contact and the second peak (F2) related to heel contact. As

the subjects increased their landing heights, the peak GRF values increased. These particular findings reveal that there is increased loading on the body with increases in either landing height or landing techniques. A further relevant finding was that they found an increase in the ankle eccentric work as the landing height increased. They also found a change of eccentric work pattern from low to high height for the hip and ankle joints in different landing techniques.

Muscle Geometry

The size of a muscle and its location relative to the joint that it crosses significantly affects the mechanics of a muscle. Since a muscle force solution is sensitive to varying muscle sizes and different definitions of physiological cross-sectional areas (PCSA), the question arises of what is the proper way to account for varying muscle sizes. Brand et al. [7] tried to determine whether or not either muscle size or definition of PCSA could significantly affect muscle force solutions. After measuring the length and angle of pennation of all muscles in two cadavers, the muscles were excised and the length of 10 - 20 muscle fibers from each muscle was measured. The PCSA was defined as the muscle volume divided by the averaged muscle fiber length. Kinematics and ground reaction forces were recorded with a film camera and force platform to calculate muscle and joint forces for selected activities. To calculate the forces in individual anatomic structures, a straight-line muscle model was used based on anatomical dissections of six cadavers. Since there are more unknown muscle forces and joint

contact forces than possible equations of motion, a mathematical technique of optimization was used to solve for individual forces. The authors calculated the muscle forces for a single gait cycle using the two PCSA values obtained from the two specimens and the PCSA value by Pierrynowski (1982). Their results showed that for a given muscle they could not predict which of the three PCSA would result in the largest muscle force because some of their muscles had the largest PCSA while some of the PCSA from Pierrynowski data set had the largest value. Therefore, they concluded that a muscle force solution could be very sensitive to PCSA.

Grieve et al. [15] provided a technique where as the length of the human gastrocnemius muscle can be estimated from angular measurements of the lower limb. Limbs of eight cadavers were excised by disarticulation at the hip or by hemisection of the pelvis. Next the limbs were dissected at the distal and mid-tarsal regions with the tendon sectioned at a level 3 cm proximal to the insertion on the calcaneus. A wooden board was nailed to the sole of the foot and pins were placed at the estimated centers of rotation of the ankle, knee, and hip joints. While one joint was stabilized the other joint was manipulated through its range of motion and measurements were taken at 10° intervals. A reference length was obtained when the knee and ankle were both at 90° . The changes in muscle lengths were expressed as deviations from this reference length. Each length was then normalized as a percentage of the shank length (distance between the assumed centers of rotation of the knee and the ankle joints). The authors fitted this data with second-order polynomials with respect to changes of ankle and knee joint positions to obtain the length of the gastrocnemius:

$$\Delta L_i = A_0 + A_1(\Theta_i) + A_2(\Theta_i)^2$$

where ΔL_i is the percent muscle length change attributable to angle Θ_i and Θ_i is the angle of the i^{th} joint (ankle or knee). The coefficients A_0 , A_1 , and A_2 can be found in Appendix C.

Herzog et al. [20] obtained lines of action and moment arms in the sagittal plane for major force-carrying structures crossing the human knee joint: quadriceps, hamstring muscles, two cruciate ligaments, and two collateral ligaments from five cadavers. First, the movement of the tibia relative to the femur was determined throughout the full range of motion for the intact knee joint. Next they determined the attachment coordinates of selected ligaments and muscles on the tibia and femur. The lines of action for each structure at each knee joint configuration were calculated. A vector directed from the insertion of the structure on the tibia to the insertion on the femur represented the lines of action for each structure. The projected angles of the vectors were then calculated using the cosine function. The authors used the perpendicular distance from the line of action of the structure about the transverse axis to the knee joint center as the moment arm. They then used a best fitting polynomial regression equation to predict the lines of action of each structure as a function of the knee joint angle:

$$\text{Line of action} = A_0 + A_1(\theta) + A_2(\theta)^2 + A_3(\theta)^3$$

where θ is the angle in degrees and A_0 - A_3 are polynomial coefficients. Similarly, the polynomial equation was generated to predict the moment arms for each structure:

$$\text{Moment Arm} = B_0 + B_1(\theta) + B_2(\theta)^2 + B_3(\theta)^3 + B_4(\theta)^4$$

where θ is the angle in degrees and B0-B4 are polynomial coefficients. Their results for predicted lines of action show a similar pattern as reported in literature. However, the moment arms predicted in this study showed similar patterns but were greater than other values reported in the literature they used for comparison.

Spoor et al. [35] determined the moment arms of lower-leg muscles as functions of joint angles for musculoskeletal modeling. They measured the tendon displacement and joint angulations on two embalmed specimens. Using the distal third of the thigh and the whole lower leg from the specimens, two methods (A and B) for measuring the muscle length change as a function of knee flexion angle were used. Knowing that when a force is at a right angle to an axis, the moment arm a is defined as the distance from the axis to the line of action of the force, and equals the ratio of moment over force. Further, when the angle α between the axis and the force is unequal to $\frac{1}{2} \pi$, the moment equals force times distance times $\sin \alpha$. Including this body of knowledge, the authors defined the effective moment arm as moment divided by force. They deduced the relationship from the equation of muscle work and joint work. Therefore the effective moment arm was:

$$a = \frac{M}{F} = \frac{ds}{d\phi}$$

where work done by a force F , over an infinitesimal tendon excursion ds equals the work done through an angle $d\phi$ by the moment M about the rotation axis of the joint. The authors compared their results with the relationship between muscle length and joint angle as given by Grieve et al. [15]. There were minimal differences in the moment arm curves predicted by their equations and the curves of the experimental data providing

validity to their equation. However the moment arms predicted by Grieve et al. [15] were much larger than those experimentally measured.

Visser et al. [38] determined the length of the human quadriceps femors muscle, biceps femoris muscle and gastrocnemius muscle as a function of lower limb joint angles. Six legs of five human cadavers were excised from the body at the level of the fourth lumbar vertebra for this study. The muscles dissected from the cadavers included the rectus femoris (RF), vastus intermedius (VI), vastus medialis muscle medial part (VMM) and lateral part (VML), and vastus lateralis muscle medial part (VLM), lateral part (VLL) biceps femoris muscle (BF), and gastrocnemius (G). Each leg was mounted in a special frame that was constructed for this study. The joint angle was changed from 0^0 to 90^0 of flexion for the knee and from -15^0 to 60^0 of the hip in 5^0 increments. A second degree polynomial was used to fit muscle length:

$$\Delta l_{oi} = A_0 + A_1 \Theta_i + A_2 (\Theta_i)^2$$

where Δl_{oi} is the origin to insertion length relative to the segment length, Θ_i is a joint angle in degrees, and A_0 , A_1 , and A_2 , are polynomial coefficients. The muscle moments arms where given as a function of knee and hip joint angles:

$$d = (A_1 + 2A_2 \Theta_i) \times 180/\pi$$

where the moment arm (d) is a percentage of segments length, Θ_i is in degrees and A_1 , and A_2 are the same constants as above. The results indicated the effect of changing the hip angle on the BF length was greater than that of changing the knee angle, however, the reverse was true for the RF. For the VML, VLM, and VI changes in length were similar while the changes in length of the VMM and the VLL were similar but differed

significantly from the VI. To examine whether biarticular muscles changes in length could be expressed as the algebraic sum of changes caused by changing joint angles they performed measurements at a hip angle of 45° . Results for the RF and BF were related. After comparing the results from with data from Grieve's study, similar findings were reported.

The basic building block of muscle is the sarcomere. More accurately, the force-length properties of muscles/muscle fibers are normally coupled with sarcomere lengths. Herzog et al. [19] determined thick and thin myofilament lengths of skeletal muscle and derived the corresponding sarcomere force-length properties using the cross bridge theory. Transmission electron microscopy was used to determine the myofilament lengths of cat, rat, and rabbit skeletal muscles. Comparison of their values of thin myofilament lengths of rat and rabbit skeletal muscle was in agreement with values reported in previous literature. They used their length values to derive the sarcomere force-length properties of frog, cat, and human skeletal muscles. The results showed that peak forces should occur between sarcomere lengths of 2.34 and 2.51 μm .

Additional Models

The Distribution Moment Model

Zahalak [42] derived a Distribution-Moment model (DM) based on the biophysical model proposed by A. F. Huxley which incorporates actin-myosin kinetics.

Using this newly derived equation, the author compared the experimentally measured behaviors of the cat soleus muscle to the predictions of the DM model.

When the author compared the dependence of the isometric moments on the bonding rate parameter, the DM produced similar predictions as the Huxley model. Also, the author compared the stiffness predicted by the Huxley model to the DM model and showed an agreement with each other within about 10 percent. The author also successfully predicted chemical energy and produced heat rates simultaneously with mechanical responses. In summary, the DM model predicts a number of mechanical behaviors observed in the cat soleus muscle under constant simulation.

Other Models

Woittiez et al. [41] examined the mechanical behavior of the Triceps Surae (TS) muscle, gastrocnemius, mediale (GM), gastrocnemius laterale (GL), and soleus (SO). It was assumed that GM, GL, and SO attain their optimal length when the knee and ankle joint are at 75° and 85° respectively. They used a three dimensional muscle model to estimate the geometrical reconstruction and functional characteristics of the TS with the typical force-length and force-velocity relationships. The results indicated that the SO produced the largest amount of maximal isometric force followed by GM and GL. The absolute muscle length was 51.8, 43.4, and 34.8 mm for GL, GM, and SO respectively. During fast walking, the range of the physiological length used was 60% for SO 90% for GM, and 75% for GL. At the optimal length, the maximal power of the muscles was found to be 69.3, 36.9, and 69.4 W respectively. The power of SO during the eccentric contraction in the first part of the stance phase is greater than the contributions of GM or

GL because of less lengthening of GM and GL due to simultaneous knee flexion. The shortening velocity is lower for SO than GM and GL.

Meijer et al. [26] developed a Hill type muscle model to account for the effects of shortening history. The *standard* Hill model consisted of a contractile element and a series elastic element:

$$F_{ce}(l_{ce}, v_{ce}) = \left(\frac{F_{ce}(l_{ce}) \cdot b - v_{ce} \cdot a}{v_{ce} + b} \right)$$

where a and b are constants, F_{ce} is the contractile element force, v_{ce} is the contractile element velocity, and l_{ce} is the length of the contractile element. The *modified model* was given by:

$$F_{ce}(l_{ce}, l_{ce(t)}, \Delta l_{ce}, v_{ce}) = F_{ce}(l_{ce}, v_{ce}) \times (1 - \Delta F_{ce}(l_{ce(t)}, \Delta l_{ce}, v_{ce}))$$

where F_{ce} is the contractile element force, v_{ce} is the contractile element velocity, and l_{ce} is the length of the contractile element. Both the results of the modified model and the standard model were compared with experimental results performed on in situ medial gastrocnemius muscle of 10 male Wistar rats. The simulated experiments included short-range isokinetic contractions with different starting lengths and different contraction speeds, isokinetic contractions with shortening amplitudes larger than those used to determine parameter values, and isotonic contractions against loads of 20-75% of maximal isometric force. Their results indicated that the modified model performed adequately in describing the force depressions where as the standard model failed to predict forces at different starting lengths and velocities. The modified model agreed well with the experimental data on isometric force redeveloped after shortening for different end lengths however it overestimated the force depression at optimum lengths.

For the same experimental protocol the standard model compared well on all accounts to the experimental data. When comparing the two models at isotonic contractions against a low and high load, the modified model more accurately predicted the time-length and length velocity curves. The standard model overestimated both shortening range and velocity. The authors concluded that the modified Hill model is better suited to describe the time history effects during short-range isokinetic contractions, non-linear length changes observed during isotonic contractions, and a depiction of force after large length changes.

Chapter III

Research Methods

Experimental Methods

Experiments were performed to explore a model for the triceps surae during landing using different techniques. The procedure for the experiment consisted of a standard warm-up, anthropometric measurements, and actual data collection. The subjects performed five trials of drop landings in each of the four conditions for a total of twenty trials.

Subjects

All subjects signed an informed consent form approved by the Institutional Review Board at The University of Tennessee before participating in the study. Ten healthy and physically active male subjects were recruited from the student population of The University of Tennessee. None of the subjects had a prior history of major injuries to the lower extremities and participated in recreational sports two to three times a week. The subjects were informed about the purpose, procedures, risks, and benefits of this study before their participation.

Instrumentation

All testing was conducted in the Biomechanics/Sports Medicine Lab, Room 135, HPER Building at The University of Tennessee. The biomechanical instruments used in

this study included a force platform, an electrogoniometer (elgon), a video camera, a trigger device, a reference frame, reflective markers, an analog/digital (A/D) converter, and an Ariel Performance Analysis System (APAS, Ariel Dynamics, Inc.) for data collection and processing.

Kinematics

The right sagittal views of the subjects were filmed using a digital video camera (GR-DVL 9800, JVC) to obtain kinematic data at 120 Hz. Six reflective markers were placed on the shoulder, hip, knee, ankle, heel, and head of the fifth metatarsal (Figure 2). In order to obtain scale factors that could convert the anatomical coordinates of the reflective markers, a reference frame (width = 140.97 cm, height = 186.69 cm) was used. On each of the four corners of the reference frame, a coplanar reflective marker was placed. The recorded video images were digitized to obtain coordinates of reflective markers.

Force Platform

The ground reaction forces (GRF) F_x , F_y , and F_z , and moments M_x , M_y , and M_z , were recorded using a force platform (OR6-7, AMTI). The GRF forces F_x , F_y , and F_z represent the medial-lateral, anterior-posterior, and vertical forces respectively. M_x , M_y , and M_z are the moments applied about the F_x , F_y , and F_z axes. The signals from the force platform were amplified through the A/D converter before being stored in the APAS computer. The sample period was set at 1.0 seconds and at a frequency of 1200 Hz.

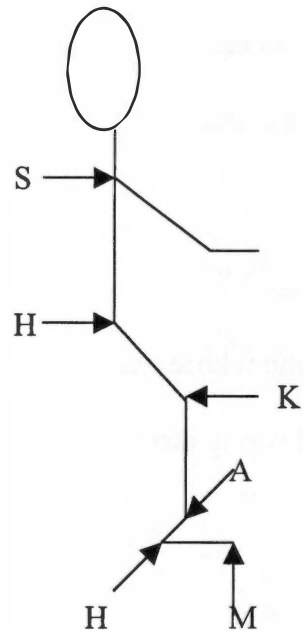


Figure 2. Positions of reflective markers at shoulder (S), hip (H), knee (K), ankle (A), heel (H), and fifth metatarsal (M).

Electrogoniometer

An electrogoniometer (Penny+Gile, 1000 Hz) was used to monitor the left knee flexion angles. A mean maximum knee flexion angle was obtained to determine the range of maximum knee flexion for each test condition [45]. The equation used to determine this range was:

$$\alpha_{range} = \alpha_{max} \pm 9^{\circ}$$

where α_{range} is the range of maximum knee flexion angle and α_{max} is the mean maximum knee flexion angle. This method was to insure that each subject was performing a consistent landing technique.

Synchronization

The force platform, the sagittal view video of the body, and the elgon were simultaneously recorded during the experiment. To accomplish synchronization between the kinematic and analog signals (the force platform and the elgon), a customized trigger device with a light emitting diode (LED) was employed during the test.

Experimental Protocol

All subjects were briefed on the purpose and the procedures of the study by the principal investigator preceding their participation in the study. Furthermore, the subjects were given information about the number of conditions, the number of repetitions, and performance requirements of the study. Including practice and familiarity with the

testing protocol, the test session lasted approximately one hour. The subjects in four conditions performed 20 trials of drop landings.

Before beginning the drop landings, each subject performed a warm-up by riding a stationary bike for five minutes at a moderate intensity. Next, anthropometric measurements including the proximal and distal circumferences and length of lower extremity segments were taken three times, (Appendix E, Table 1) and the mean value was determined for further analysis. A mathematical anthropometric model was used to estimate inertia characteristics and the center of gravity (COG) of each lower extremity segment [17].

Following the anthropometric measurements, reflective markers were placed on the acromioclavicular joint, the greater trochanter, the knee joint, and the lateral malleolus the heel and the head of the 5th metatarsal of the right side of the body.

Each subject will land from a height of 0.60 m, using four different landing techniques. Before the actual collection of data, the subjects were instructed about the landing techniques and the practice of each technique was required. The subjects were asked to perform landings in four different conditions (techniques): (1) a normal landing that consisted of a landing technique in which the subject would utilize in a sporting event (NL); (2) a stiff landing that required the subject to perform the same type of landing as before but with minimal knee flexion (SL); (3) a SL but landing flat footed (SF); (4) and a stiff landing while landing on the toes only and contracting the calf muscles (SC).

The overhead drop bar was adjusted to accommodate each subject's height so that each subject was landing from a height of 0.60 m measured from the calcaneus to the

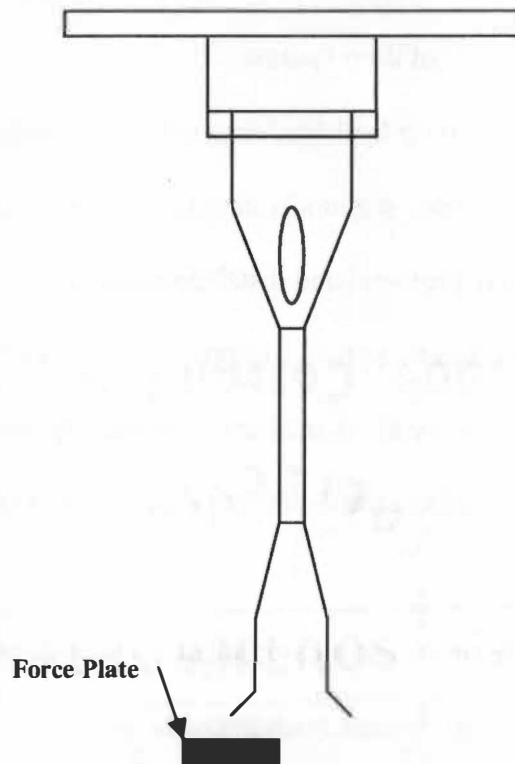


Figure 3. Drop Setup

landing surface (i.e. the force platform). The subjects were instructed to perform their respective drop landings with only the right foot landing on the force platform and the left foot on the adjacent floor flush with the force platform. The setup is shown in Figure 3.

Data Processing

The digital video that was obtained during data collection was processed in four steps. First, 120 frames of video images was captured and stored for each trial on the

APAS system. Of the 120 frames, 20 frames included what occurred before foot contact and the remaining 100 frames demonstrated what happened after foot contact. The next step was to digitize the reflective markers using the APAS system. Also included in this second step was to digitize the reference frame in order to acquire scale factors to convert the coordinates of digitized reflective markers from a screen reference system to a lab reference system. In the third step a customized computer program was used to decode, smooth, and reconstruct the digitized coordinates. The digitized coordinates were smoothed using an algorithm to obtain optimal cutoff frequencies individually for x and y coordinates of each reflective marker [23]. A Shannon algorithm was used to reconstruct the video signal from 120 Hz to 240 Hz [16]. In the fourth step, linear and angular kinematic variables and corresponding discrete events were computed or determined using a second customized program.

The force platform data collected were analyzed in two steps. The first step was the decoding of the analog file stored on the APAS system using a customized program to obtain time history of GRF data and stored in an ASCII format. Secondly, the decoded analog file was imported into another customized program to determine and compute GRF variables. These variables included the first (F1) and second (F2) maximum vertical GRF, times associated with F1 and F2, and impulse computed from touchdown to 100 ms.

Calculation of Center of Gravity (COG)

The center of gravity (COG), inertia, and properties of each body segment are all calculated using the anthropometric dimensions of the individual subject using an

mathematical anthropometric model proposed by Hanavan [17], where the model of the leg and foot is a frustrum of a right circular cone. The symbols and equations representing the dimensions and properties of the leg and foot are found in Appendix E. The moment of inertia of each body segment can be determined by

$$I = \frac{2AAM^2}{\Delta SL}$$

where M is the mass of the body segment, ΔSL is the change in the length of the segment, and A is the frusta of right circular cones.

Joint Kinetics and Muscle Model

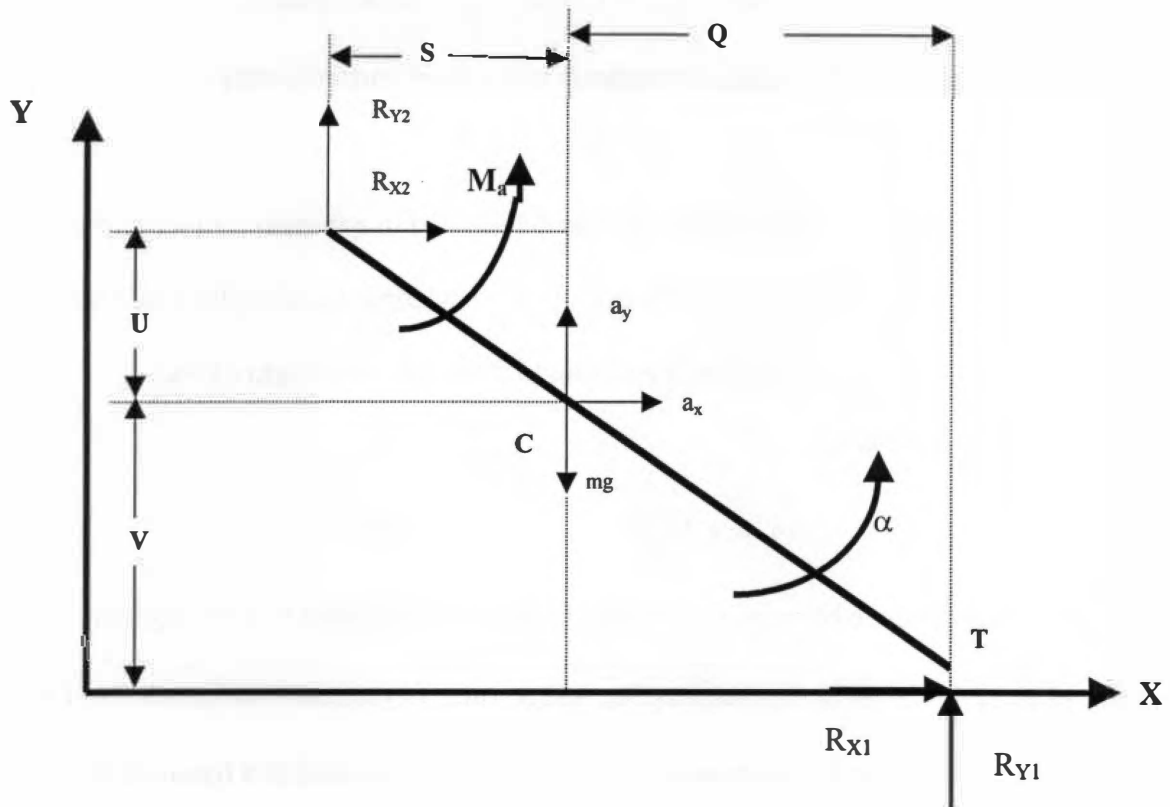
After processing kinematic and kinetic data, the resultant moment about the ankle was calculated for each subject using an inverse dynamics approach [39] and by solving equations of motion of the foot (Figure 4). After obtaining the ground reaction forces from the force platform, reaction forces at the ankle joint in the x (R_{x2}) and y (R_{y2}) direction were determined by the following equations:

$$R_{x_2} = ma_x + R_{x_1} \quad (1)$$

$$R_{y_2} = ma_y - mg + R_{y_1} \quad (2)$$

where R_{x1} and R_{y1} are the ground reaction forces in the x and y directions and a_x and a_y are the linear acceleration of the foot in the x and y directions. Next the moment about the ankle [44] was calculated using the following equation:

$$M_a = I_o\alpha + R_{x_1}V + R_{y_1}Q - R_{y_2}S - R_{x_2}U \quad (3)$$



Where:

a_x and a_y are the components of linear acceleration in x and y direction

mg is the weight of the foot

α is the angular acceleration

R_{X1} and R_{Y1} are the ground reaction forces in the x and y direction respectively

R_{X2} and R_{Y2} are the reaction force at ankle joint in the x and y direction respectively

C is the center of mass of foot

M_a is the moment about the ankle joint

Q , S , U , and V are the components of moment arms of forces

Figure 4. Free body diagram of the foot, and equations for calculation of dorsi-flexing moment.

where I_0 is the moment of inertia about COG of the foot, α is the angular acceleration of the foot, and Q, S, U, and V are the components of moment arms associated with the ankle.

The moment arm of the calf muscle was determined in a manner similar to that described by Bobbert et al. [4] and Visser et al. [38]. A second-degree polynomial was implemented in a customized computer program to determine the length of the gastrocnemius and the soleus:

$$\Delta l_{oi} = A_0 + A_1 \Theta_i + A_2 (\Theta_i)^2 \quad (4)$$

where Δl_{oi} is the distance between the origin and the insertion relative to the segment length, Θ_i is a joint angle in degrees, A_0 , A_1 , and A_2 , are polynomial coefficients and I is the i^{th} joint (ankle or knee). The muscle moment arm was estimated as a function of ankle joint angles by the following equations [38]:

$$d = (A_1 + 2A_2 \Theta_i) \times 180 \pi \quad (5)$$

where the moment arm d is a percentage of segment length, Θ_i is in degrees, and A_1 and A_2 are the same polynomial coefficients in (4).

The eccentric muscle force generated by the calf muscle was estimated using the following equation [9]:

$$\dot{L}_{CE} = -L_{CE(OPT)} \left[(F_{CE} / F_{MAX} + c_2)^{c_1} + c_3 \right] \quad (7)$$

where $L_{CE(OPT)}$ is the same parameter as described above, F_{MAX} is a constant, F_{CE} is the force of the contractile element (i.e. the calf muscle), and c_1 , c_2 , and c_3 are parameters used to describe the shape of the hyperbolic curve. The right hand side of the

differential equation was solved for at each time step and then integrated using a simple Euler method (MATLAB software, The MathWorks, Inc., Natick, MA). The details of the model are described in Appendix F.

Following calculation of the estimated moment arm and muscle force, the estimated moment about the ankle was computed. The estimated moment about the ankle is then compared to the actual moment obtained from the experimental results.

The variables evaluated for VGRF included the peak associated with toe contact (F1), the minimum Force produced (Fmin), the peak associated with heel contact (F2), time to F2 (T2), the loading rate of F1 (LrateF1) and F2 (LrateF2), impulse, the maximum braking force (MaxBrF), time to maximum braking force (TmaxBrF), maximum propulsion (Mprop), and time to maximum propulsion (TmaxProp). The values assessed for the kinematic variables of the three lower extremity joints included contact angle at ground contact, maximum joint angle, time to maximum joint angle, range of motion (ROM), angular joint velocity at ground contact, and angular joint maximum velocity. A one-way analysis of variance (ANOVA) was used to compare the differences between the means for each variable during each condition. The significant level for difference was set at $P < 0.05$. Statistical analysis was performed with SPSS for Windows (SPSS, Chicago).

Chapter IV

Biomechanical Behaviors of the Human Triceps Surae

During Landing Activities

Introduction

Eccentric muscle actions play a vital role in sport activities especially in sports involving landing activities. In a landing activity, the gastrocnemius and soleus have been shown to be an important part of the impact absorption process [2, 3, 5].

Typically in a concentric contraction, a skeletal muscle develops tension as the shortening velocity increases, however in an eccentric contraction if too great of a resistance is applied to the muscle it lengthens but only after producing more tension. In an eccentric contraction, if immediately after the binding of actin and myosin filaments occurs and the cross-bridge is forcibly pulled backward, the actin-myosin bond breaks before the transfer of energy can occur [36]. Thus, from this forced muscle lengthening the muscle becomes more susceptible to injury. Many studies have factually documented that an injury occurs to a muscle after eccentric exercises. Garret et al. [13] reported that muscle strain injuries occur most often during eccentric muscle contractions and that biarticular muscles are more at risk for such an injury. Friden et al. [12] demonstrated a total disruption in the myofibrillar Z-bands after as many as six days following bouts of eccentric exercise. Further studies have reported elevated plasma creatine kinase (CK) values, connective tissue damage, and changes in the excitation-contraction coupling process after subject's performed bouts of eccentric exercises [8, 27, 37]. Other studies

have shown that strength training with an accentuated eccentric component or eccentric only training provides no gain in concentric strength and limits the amount of concentric peak torques that can be produced and even causes motor impairment [14, 22, 24, 25].

Muscle models can be used to study the contractile behaviors of muscles in an effort to better understand the injury mechanism. In an often cited study, Hill [21] concluded that skeletal muscle is composed primarily of a contractile element (CE), which is where the active force is generated and an elastic element in series (SE) with CE [11]. Several types of muscle models can be used to study the biomechanical behavior of muscles including the Huxley model which is based on the binding and unbinding of actin and myosin myofilaments [43]; the Distribution Moment Model, which is used frequently for the quantification of heat production and energetics [42]; and the Hill model which is universally accepted by engineers and biologists as an appropriate representation of muscle mechanics [21]. The Hill model is most advantageous for studying contractile behavior of muscles because the CE, SE, and properties of the tendon can be readily determined [10].

Muscle models have been used extensively to investigate numerous types of human movement ranging from finger mechanics to spinal forces [28, 34]. However, a large body of the literature on muscle modeling includes topics on jumping and concentric muscle actions [1, 4, 6, 29, 31-33]. Typically, these research studies examine the role of concentrically contracting muscles or simulate muscles only undergoing concentric contractions. Pandy et al. [29] constructed an optimal control Hill type model for studying maximum height jumping. The model allowed them to simultaneously synthesize the time histories of segmental motions, muscle forces, muscle activations,

and incoming neural control. Bobbert et al. [4] used a Hill type model to study how the human triceps surae muscle-tendon complex behaves during plantar flexion in jumping. Using a Hill type model, Soest et al. [32] determined a single selected stimulation pattern of muscles works for a wide range of starting positions for the successful performance of a squat jump. Very limited research is provided on muscles undergoing eccentric muscle contractions. Cole et al. [9] compared the force-time responses of maximally activated muscle during iso-velocity stretches at different velocities using a Hill type model and the DM. Upon comparison to the experimental data, the Hill model provided a good prediction of the kinetic response to slow and fast stretch of maximally stimulated muscle. Also, the research does not combine landing activities when investigating the biomechanical characteristics of muscles undergoing eccentric contractions. Instead, landing studies such as Self et al. [30] focus on maximum vertical ground reaction forces, maximum tibial acceleration, and ankle kinetics using four types of landing techniques. Further, Zhang et al. [45] investigated changes in energy absorption of lower extremity joints for different landing heights and techniques. Therefore, the purpose of this study is to investigate the biomechanical behaviors of the human triceps surae in landing activities using a Hill type model. Additionally, the following hypotheses were tested: (1) ground reaction force (GRF) peak will be significantly lower for stiff-legged, flat-footed landing techniques than toe-heel landings; (2) the forces generated in the calf muscles will be greater for toe-heel and toe-only landings than for stiff-legged flat footed landings; (3) the moment about the ankle will be larger for stiff-legged landing techniques than toe-heel landings.

Methods

Subjects and Experimental Protocol

Ten healthy and physically active males (age: 23 ± 3 yr, height: 1.80 ± 0.08 m, body mass: 74 ± 7.4 kg, see Appendix G, Table 3 for individual data) were recruited from the student population. All subjects signed an informed consent form approved by the Institutional Review Board at The University of Tennessee prior to their test sessions. All subjects had no prior history of major injuries to the lower extremities and participated in recreational sports two to three times a week.

After warming up, the subjects performed five trials of drop landings in each of four conditions: a normal landing (NL); a stiff landing that required the subject to perform a NL but with minimal knee flexion (SL); a SL but landing flat footed (SF); and a stiff landing while landing on the toes only (SC). Before beginning the data collection a mean maximum knee flexion angle was obtained using an electrogoniometer (Penny+Giles, 1000 Hz) to determine the maximum knee flexion angle for each landing technique [45]. To obtain the maximum knee flexion angle, each subject performed three drop landings for each condition prior to the test session and an average for each condition was calculated. If the subject failed to achieve the maximum knee flexion angle $\pm 9^{\circ}$ [45] during the test session then the trial was repeated. Using four different landing techniques, each subject landed from a height of 0.60m which was determined from the heel of the subject to an overhead drop bar.

Instrumentation

The right sagittal view of the subjects was filmed using a digital video camera (GR-DVL 9800, JVC) to obtain the right sagittal kinematic data at 120 Hz. Six reflective markers were placed on the shoulder, hip, knee, ankle, heel, and head of the fifth metatarsal. In order to obtain scale factors that could convert the anatomical coordinates of the reflective markers, a reference frame was used. The recorded video images were digitized to obtain coordinates of reflective markers. Simultaneously, the ground reaction forces (GRF) F_x , F_y , and F_z , and moments M_x , M_y , and M_z , were recorded using a force platform (OR6-7, AMTI) and sampled for 1.0 seconds and at a frequency of 1200 Hz. The signals from the force platform were amplified through an A/D converter before being stored in the Ariel Performance Analysis System (APAS). Synchronization between the kinematic and analog signals (force platform and the elgon) was accomplished using a customized trigger with a light emitting diode (LED).

After digitization of the reference frame, 120 frames were digitized for each trial. The digitized coordinates were smoothed using an algorithm to obtain optimal cutoff frequencies individually for x and y coordinates of each reflective marker [23]. A Shannon algorithm was used to reconstruct the video signal from 120 Hz to 240 Hz [16] after which linear and angular kinematic variables and corresponding discrete events were determined. Signals from the force plate were decoded to obtain the time history of the GRF data and stored in an ASCII format. The decoded analog file was used to determine the first (F1) and second (FMAX) maximum vertical GRF, times associated with F1 and FMAX and impulse computed from touchdown to 100 ms.

The center of gravity (COG), inertia, and properties of each body segment were all calculated using the anthropometric dimensions of the individual subject using a mathematical anthropometric model proposed by Hanavan [17].

Joint Kinetics and Muscle Model

After processing kinematic and kinetic data, the resultant moment about the ankle was calculated for each subject using an inverse dynamics approach [39] and by solving equations of motion of the foot.

The moment arm of the calf muscle was determined in a manner similar to that described by Bobbert et al. [4] and Visser et al. [38].

The eccentric muscle force generated by the calf muscle was estimated using the following equation [9]:

$$\dot{L}_{CE} = -L_{CE(OPT)} \left[\frac{c_1}{(F_{CE} / F_{MAX} + c_2)} + c_3 \right] \quad (7)$$

where $L_{CE(OPT)}$ is the velocity of shortening for the calf muscle, F_{MAX} is a constant, F_{CE} is the force of the contractile element (i.e. the calf muscle), and c_1 , c_2 , and c_3 are parameters used to describe the shape of the hyperbolic curve. The right hand side of the differential equation was solved for at each time step and then integrated using a simple Euler method (MATLAB software, The MathWorks, Inc., Natick, MA). A more detailed account of the model is provided in Appendix F.

Following calculation of the estimated moment arm and muscle force, the estimated moment about the ankle was computed. The estimated moment about the ankle was then compared to the actual moment obtained from the experimental results.

The variables for VGRF included the peak associated with heel contact (FMAX), the loading rate of FMAX (Lrate), and the maximum braking force (MaxBrF). The kinematic variables of the three lower extremity joints included maximum joint angle (Max), range of motion (ROM), and angular joint maximum velocity (MaxVel). A one-way analysis of variance (ANOVA) was used to evaluate selected variables with the significant level set at $P < 0.05$ (SPSS, Chicago).

Results

For the hip joint MAX in NL was significantly greater than SL or SC (Table 4). ROM was significantly greater than SL and SF. MaxVel for NL was greater than SL. For the knee joint Max for NL was significantly greater than the other landing conditions. ROM for NL was greater than SL and SF. Knee MaxVel decreased significantly from NL to SL, increased significantly from SL to SF, and decreased significantly from SF to SC. As for the ankle joint, MAX for NL was significantly greater than SL and SC. ROM and MaxVel for SF were significantly smaller than all other three conditions (for representative curves of the three lower extremity joints' angles and velocities, see Appendices I-N, Figures 5-10 and for complete data table and individual subject means and standard deviations, see Appendices O-T, Tables 7-12).

A typical time-history curve of the vertical ground reaction force for each condition is shown in Figure 11. A distinct peak associated with heel contact was seen in all four conditions. FMAX increased significantly with increasing landing stiffness

Table. 4 Means and standard deviations of angular kinematic variables for the three joints of the lower extremity.

Joint	Condition	Max	ROM	MaxVel
Hip	1 (NL)	70.94 (2.15)	47.49 (1.87)	311.76 (13.97)
	2 (SL)	38.96 ^a (3.53)	20.38 ^a (2.86)	210.21 ^a (17.59)
	3 (SF)	44.61 (3.12)	23.79 ^a (2.03)	265.40 (16.60)
	4 (SC)	49.52 ^a (23.24)	30.03 (24.13)	221.33 (138.78)
Knee	1 (NL)	93.12 (2.54)	59.78 (1.45)	493.26 (8.67)
	2 (SL)	67.24 ^a (2.07)	40.66 ^a (2.22)	440.28 ^a (24.49)
	3 (SF)	69.15 ^a (1.96)	38.10 ^a (1.43)	490.02 ^b (12.51)
	4 (SC)	75.78 ^a (19.88)	45.36 (20.19)	400.31 ^c (82.85)
Ankle	1 (NL)	29.93 (4.90)	41.90 (4.73)	506.59 (28.52)
	2 (SL)	23.52 ^a (0.94)	37.85 (3.04)	493.78 (38.62)
	3 (SF)	23.81 (1.10)	22.76 ^{a,b} (3.18)	309.94 ^{a,b} (45.74)
	4 (SC)	17.67 ^a (2.50)	38.28 ^c (2.76)	529.24 ^c (24.82)

Note: Angle and ROM units are in degrees.

Velocity unit is in deg/s.

Standard deviation values are in parenthesis.

The definitions of variables are in Appendix U.

^a denotes significant difference from the normal landing (NL) condition 1.

^b denotes significant difference from the stiff landing with minimal knee flexion (SL) condition 2.

^c denotes significant difference from the stiff landing but landing flat footed (SF) condition 3.

SC is a stiff landing but landing only on the forefoot and contracting the calf muscle.

Table 5. Condition means and standard deviations of VGRF.

Condition	FMAX	Lrate	MaxBrF
1 (NL)	57.39 (4.85)	1478.63 (265.83)	-14.04 (0.85)
2 (SL)	77.65 ^a (3.72)	2093.18 (403.88)	-15.58 (0.77)
3 (SF)	104.80 ^{a,b} (7.75)	5188.54 ^{a,b} (1461.43)	-18.96 (4.16)
4 (SC)	47.30 ^{b,c} (3.08)	865.26 ^c (83.72)	-10.71 ^{a,b,c} (0.78)

Note: Force (FMAX) unit is in N/kg and time unit is in seconds.

Loading rate (Lrate) unit is in N/kg/s.

Maximum breaking force (MaxBrF) unit is in N/kg

Standard deviation values are in parenthesis.

^a denotes significant difference from the normal landing (NL) condition 1.

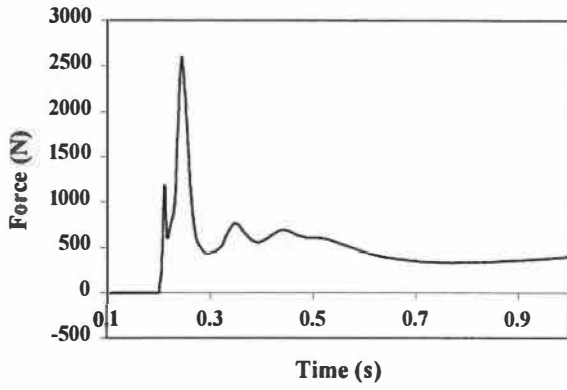
^b denotes significant difference from the stiff landing with minimal knee flexion (SL) condition 2.

^c denotes significant difference from the stiff landing but landing flat footed (SF) condition 3.

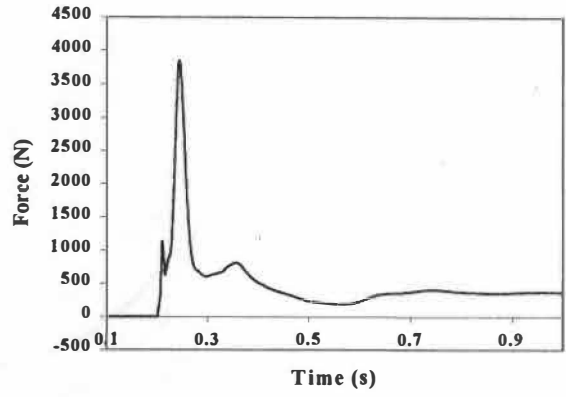
SC is a stiff landing but landing only on the forefoot and contracting the calf muscle.

techniques from NL to SF, except for SC, which was not different from NL and landing stiffness (Table 5). Similarly, Lrate increased significantly with landing stiffness except for the difference between NL and SL. MaxBrF increased in magnitude as landing stiffness increased, however only SC was significantly smaller than the other three conditions. Also, for all three variables assessed, SF had the highest values (for complete data table, see Appendix H, Table 6).

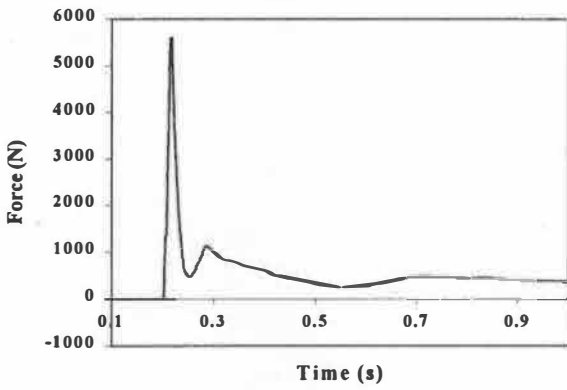
Figure 12 shows representative ensemble curves of the estimated force and the experimental force of the calf muscle for all four conditions. After touch down, the experimental force curves general did increase in magnitude from NL to SC. However, SF had the lowest mean peak value of experimental force and SC had the highest mean peak value.



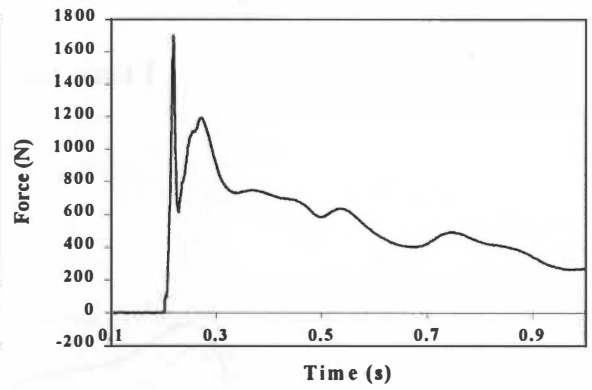
(a)



(b)

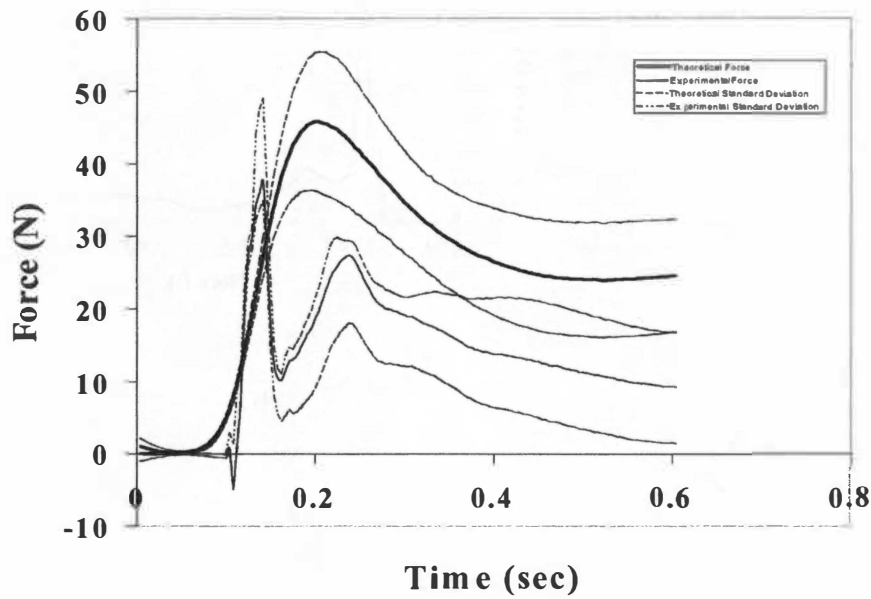


(c)

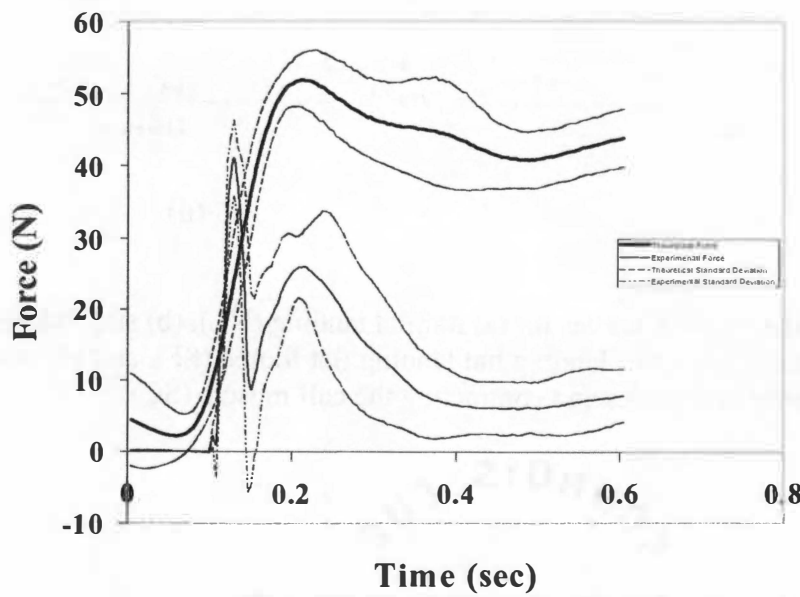


(d)

Figure 11. Representative GRF curves for (a) normal landing (NL), (b) stiff landing with minimal knee flexion (SL), (c) stiff landing but landing flat footed (SF), and (d) stiff landing but landing only on the toes and contracting the calf muscle (SC).

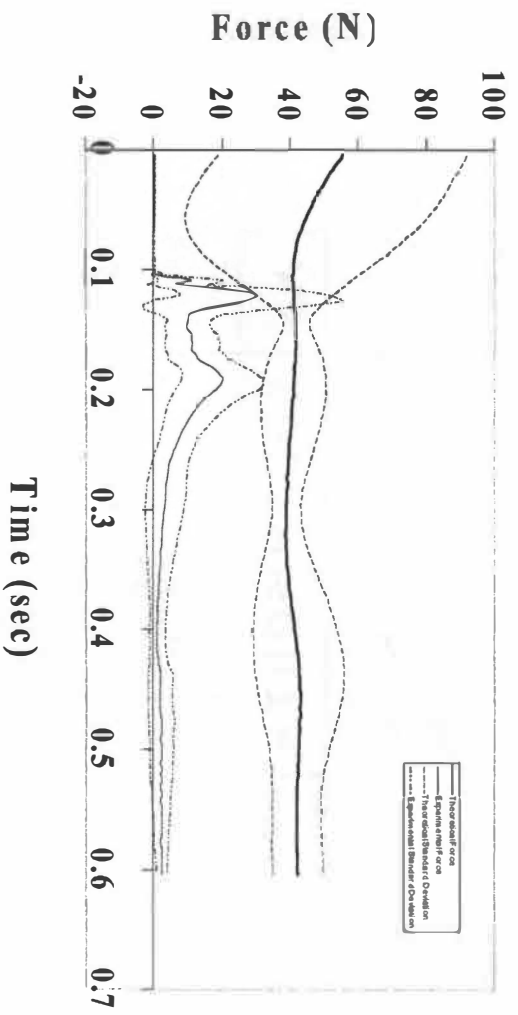


(a)

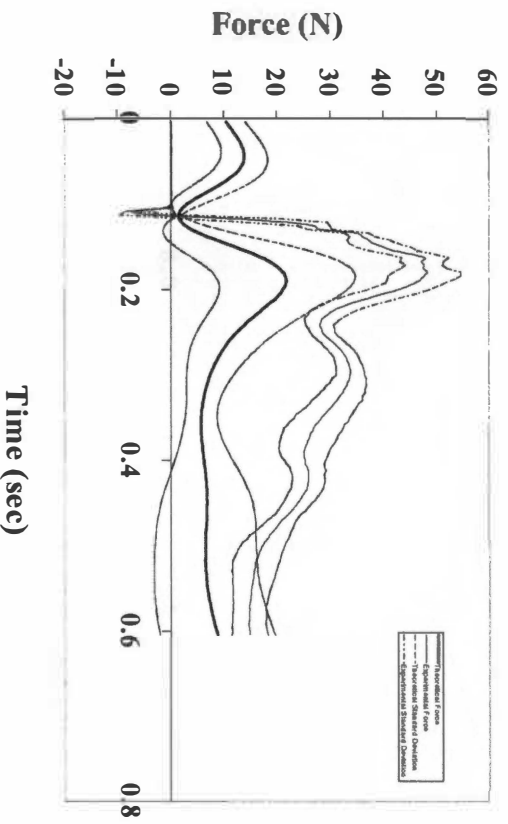


(b)

Figure 12. Representative ensemble curves of estimated and experimental triceps surae forces from one subject for (a) normal landing (NL), (b) stiff landing with minimal knee flexion (SL), (c) stiff landing but landing flat footed (SF), and (d) stiff landing but landing only on the toes and contracting the calf muscle (SC).

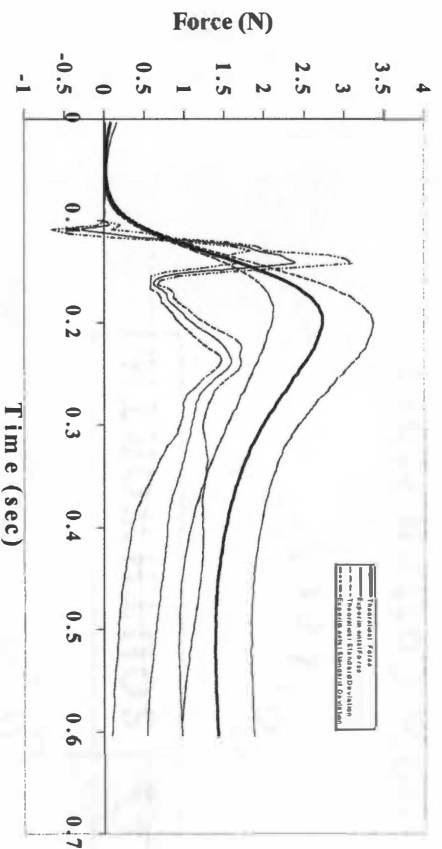


(c)

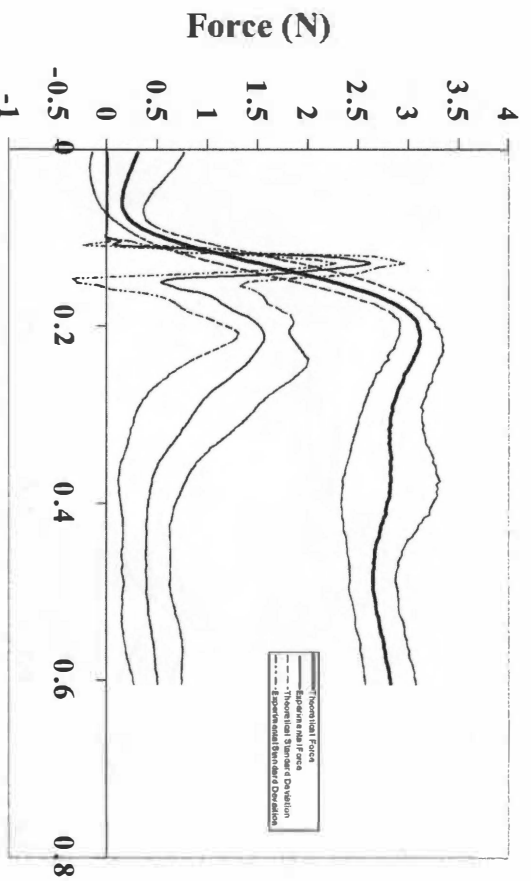


(d)

Figure 12. (Continued).

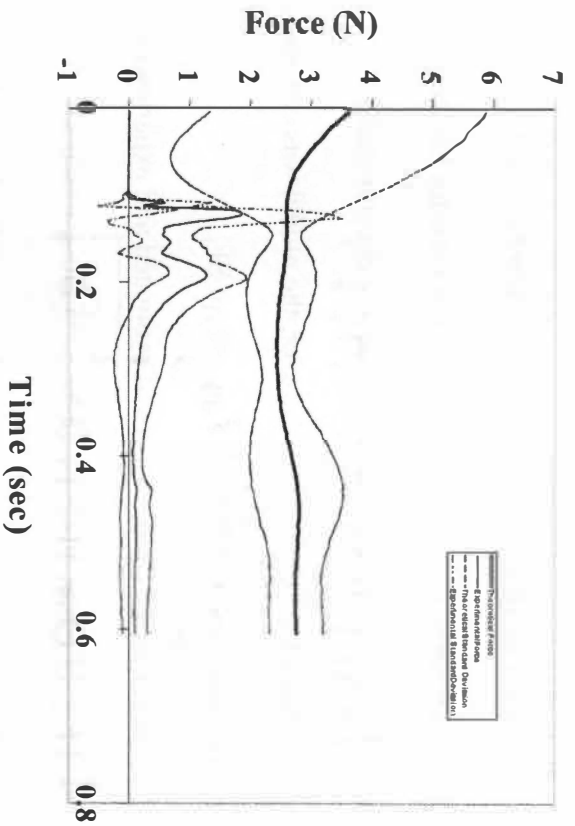


(a)

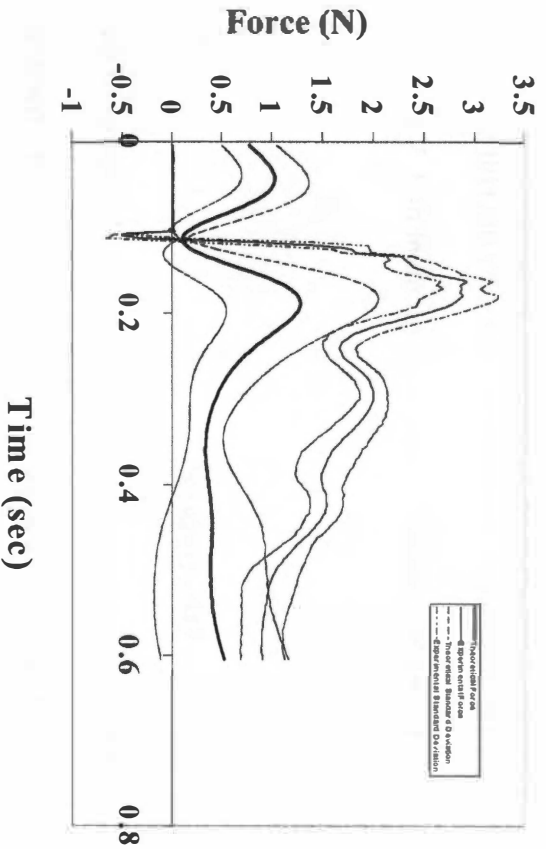


(b)

Figure 13. Representative ensemble curves of estimated and experimental triceps surae moments from one subject for (a) normal landing (NL), (b) stiff landing with minimal knee flexion (SL), (c) stiff landing but landing flat footed (SF), and (d) stiff landing but landing only on the toes and contracting the calf muscle (SC).



(c)



(d)

Figure 13. (Continued).

For NL, SL, and SC the theoretical muscle force curves have the same shape of the rectangular hyperbola first described by Hill [21]. The force predicted by the Hill model was similar to the experimental for force for NL, SL and SC. However, for SF the typical rectangular hyperbola pattern was not observed. The Hill model over estimated for NL and SL, but underestimated the force for SC overall. However, the model was considered to be a good predictor of the muscle force for all conditions except SF.

Figure 13 depicts representative ensemble curves of estimated and experimental ankle moments of one subject for all four conditions. Increases in magnitude as the landing stiffness increased in the ankle are similar to the trend seen in the force. There was an increase in the mean peak values of the moment as landing technique increased, except for that SF had the lowest value. The average experimental peak moment (obtained from the ensemble curves) for all subjects for NL, SL, SF, and SC was 2.2, 4.0, 2.8, and 4.4 Nm respectively. The product of the force calculated by the Hill model and the moment arm for NL, SL, SF, and SC yielded a mean peak moment of 3.7, 4.6, 4.7, and 3.2 Nm.

Discussion

The purpose of this study was to investigate the biomechanical behaviors of the human triceps surae in landing activities using a Hill type model. Specifically, the peak GRF peaks, the forces generated in the calf muscles, and the moment about the ankle were examined. It has been demonstrated by Zhang et al. [45] that changes in landing stiffness are closely related to changes in mechanical demands placed on the body during

corresponding responses are observed in the musculature of the lower extremities.

Further, other studies have shown that when a muscle performs an eccentric contraction an injury is likely to occur [8, 12-14, 22, 24, 27, 36, 37]. These responses can be examined by assessing changes in landing techniques in relation to the muscle force produced. The highest vertical ground reaction forces were observed during the flat-footed stiff landing in this study. The magnitude of the VGRF decreased as landing technique stiffness decreased, with the stiff landing having the second highest VGRF peaks observed followed by the normal landing. The toe-only stiff landing had the lowest VGRF peaks observed.

The findings of this study concur with Zhang et al. [45] who demonstrated that with increases in landing technique stiffness there was an increase in ground reaction force magnitudes. Additionally, this study supports the findings of Self et al. [30] when comparing differences among VGRF peaks with similar landing techniques. Self et al. [30] found a significant increase between peak GRF as stiffness increased for a normal landing, a stiff landing, and a stiff flat-footed landing. They also reported a significant difference between a stiff landing, a stiff flat-footed landing, and a stiff toe-only landing. There was a significant difference between their stiff flat-footed landing and a stiff toe-only landing. However, the magnitude of the peak GRF between Self 's [30] and this study were smaller than the peak GRF for this study. This can be attributed to experimental design and the height from which the subjects dropped. In the present study, subjects were instructed to drop from an overhead bar at a height of 60 cm while in the study by Self and Paine the subjects were dropped from a height of 30.48 cm. Also, in their study for the toe-only landing the subjects were instructed to land with minimal

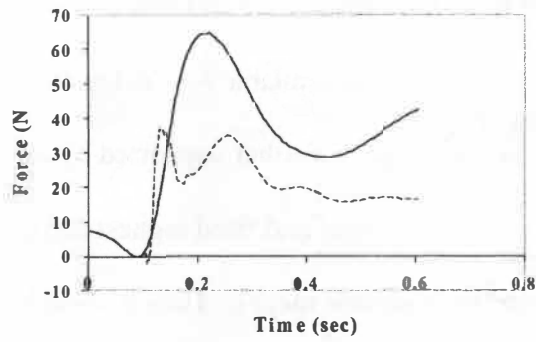
in their study for the toe-only landing the subjects were instructed to land with minimal knee flexion while “absorbing the impact through [their] toes and by flexing their calf-muscles” [30]. In the present study subjects were asked to perform a toe-only landing with minimal knee flexion. It was felt that the instructions given by Self et al. [30] would cause the subjects to alter their landing and, for the purposes of this study cause a shortened calf length measurement which in turn would underestimate the force predicted by the model. In addition, Self et al. [30] used a single-axis accelerometer attached below the knee along the long axis of the bone to estimate the Achilles tendon force. This method was not used in this study because it was felt that the tendon displacement during the calf muscle contraction would cause erroneous measurement of acceleration of the attachment sight and therefore erroneous estimation of the muscle force.

The stiff landing technique in this study indicates that the subject landed with as minimal knee flexion without locking the knees. The normal landing had the highest maximum joint angle and range of motion at the hip, knee, and ankle joints. The toe-only stiff landing had the second highest maximum joint angle and range of motion at the three lower extremity joints. Thus it seems logical that the toe-only landing requires more flexion so it can attenuate impact forces.

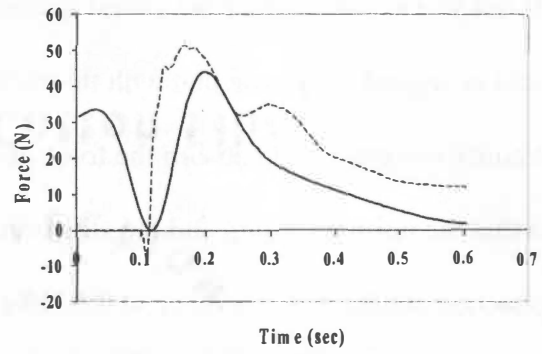
Another explanation that the lowest VGRF was observed during SC was because of the energy absorbing characteristics of the plantar flexors. The energy absorbed by the calf muscles highest in magnitude was occurred during the toe-only stiff landing (Figure 12). The next highest force produced occurred during the normal landing, followed by stiff landing, and the stiff flat-footed landing. This would suggest that the calf muscle is an important part in attenuating force in the toe-only condition. Additionally, since the

stiff flat-footed landing had the lowest amount of force produced in the calf muscles it would be logical to assume that with this technique less time is available for the lower extremity musculature to absorb the force of the impact. This is further supported by the fact that the normal landing and the stiff landing have the second and third highest force production and have a difference of 2.5 N/kg from the ensemble means. Thus it could be assumed that there was an increase in the amount of eccentric work performed by the ankle musculature as landing technique stiffness increases.

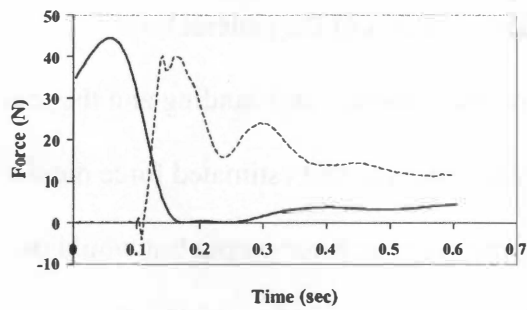
The Hill model was considered to be a good predictor of the general force response exerted by the calf musculature for the normal landing, stiff-landing and the toe-only stiff landing. Figure 14 displays the typical experimental and estimated force output from one subject. The model did a good job of estimating the force output but would in some instances overestimate or underestimate the actual force produced. The figure represented an overestimation (SC), average prediction (SC), and underestimation of force output (SC), which was considered to be a consistent representative example of how the model predicted force. In Figure 14a the modeled force overestimated the actual force. After contact, the predicted muscle force has a drastic increase in magnitude when compared to the experimental force curve. Figure 14b illustrates how the model actually performed for all subjects the majority of the time. After contact the experimental and theoretical force curves follow a similar shape and reach similar magnitudes and then declines steadily. Figure 14c exhibits an example when the model completely underestimates the force produced in the calf musculature. The curve fails to approach the asymptotic value and never actual takes the form of the hyperbola described by Hill [21].



(a)



(b)



(c)

Figure 14. Representative curves from a single subject that depicts examples of (a) overestimated force output (b) average force output (c) underestimated force output calculated by the Hill model for SC.

In order to explain some of these discrepancies it may prove beneficial to describe how the model works. The model used in this study is a function of changes in the length of the contractile element and the muscle tendon length, i.e. the length of the calf muscle. For the Hill model when the simulation begins, an initial stretch is applied to the series elastic element, which results in a force that is balanced in the contractile element [9]. Initial increases in force above the isometric force causes small lengthening velocities of the contractile element which when integrated, result in small stretches of the contractile element [9]. Finally, when the series elastic element is stretched, the force produced approaches the asymptotic value and increases in force causing large increases in velocity [9].

Some of the inconsistency observed in the subjects can be explained by oversight in experimental design. Subjects were instructed to hang from an overhead drop bar and land on the force platform using the appropriate technique. However, prior to the landing there was no instruction given on how to position the foot while suspended. Thus the subjects' ankle angle varied from trial to trial and condition to condition. As a result, the reference or starting point for the ankle angle and calf muscle length varied in the model when simulation began. The random position of the ankle angle is believed to account for large amounts of force seen in the theoretical force and moments prior to foot contact. If the subject's foot is near or completely plantar flexed for the time duration prior to touchdown, then the resultant force computed by the model is at or near maximum (Figure 14c and 14d), because force is a function of the length of the muscle. If the subjects had been required to maintain a constant ankle angle prior to touchdown, then

the force output predicted by the Hill model would have been more consistent even though the model would still depict a muscle force prior to touchdown.

As suggested by Bobbert and his colleagues [4] the difference in time histories observed in all four conditions may be credited to the influence of muscle excitation. In a study by Soest et al. [32], they used a Hill type model that accounted for neural input and a Hill type model that did not compensate for neural input. They concluded that the model that incorporated neural stimulation was a better predictor of muscle force for a vertical jumping task. In this study, the level of excitation was kept constant. The typical muscle force response was delayed after touchdown and then there were increases in muscle force (Figure 14b). It is understood that this time lag between the start of the experimental force and the beginning of the theoretical force at touchdown is because the Hill model used did not account for muscle excitation. In addition, some of the more recent studies employed optimization techniques that enhanced the performance of the Hill model [9]. It is assumed that if optimization were used for this study or optimized parameters were incorporated into the Hill model, a better agreement between the theoretical and experimental force and moment curves would be found.

For the stiff-legged flat-footed (SF) condition, the Hill model was not considered to be a good predictor of the general force response. This is due to the landing technique itself, which required subjects to land flat-footed as stiff as possible. Some subjects had a better success rate of adhering to this protocol than others. Several subjects reported that the technique was difficult to perform without enduring pain. Subsequently, the subjects were instructed to perform the landing as stiff as possible without injuring themselves by flexing the knee slightly more while landing. These subjects contributed to the wide

standard deviation bands for the computed force and moment curves, (Figures 12 and 13), and took on more of the shape of the hyperbola. These subjects used more of a toe heel landing thus the resultant ankle angle caused for a longer calf muscle length to be used in the model, which generated a higher force. The subjects who performed the technique as instructed landed more flat-footed thus causing very little change in calf muscle length. This evidence is supported by the fact that this condition had the lowest range of motion at the knee (38.10°) and at the ankle, (22.76°) when compared to the other conditions. Therefore, when using Grieve's methods [15] to calculate the calf muscle length, there will be minimal changes in muscle length and consequently very little change in muscle force predicted.

In summary, the VGRF observed in this study was agreeable with the literature. There was a significant difference between the mean peak GRF for all conditions except the normal landing and the stiff toe-only landing. It was noted this landing technique had the highest amount of experimental force observed in the calf muscle. Thus, it was concluded that as the landing technique stiffness increase there is an increase in the amount of eccentric work the ankle musculature must perform. The Hill model was considered to be a good predictor of the calf muscle force for the normal landing, stiff normal landing and the toe-only landing. The disparity seen between these conditions and the stiff flatfooted landing can be attributed to the subjects' ankle posture at contact, muscle excitation level and lack of using an optimization technique.

LIST OF REFERENCES

LIST OF REFERENCES

1. Bobbert, M.F., et al., *Why is countermovement jump height greater than squat jump height?* *Medicine and Science in Sports and Exercise*, 1996. **28**(11): p. 1402-1412.
2. Bobbert, M.F., P.A. Huijing, and G.J.V.I. Schenau, *Drop jumping I. The Influence of Jumping Technique on the Biomechanics of Jumping.* *Medicine and Science in Sports and Exercise*, 1987. **19**(4): p. 332-338.
3. Bobbert, M.F., P.A. Huijing, and G.J.V.I. Schenau, *Drop Jumping II. The Influence of Dropping Height on the Biomechanics of Drop Jumping.* *Medicine and Science in Sports and Exercise*, 1987. **19**(4): p. 339-346.
4. Bobbert, M.F., P.A. Huijing, and G.J.V.I. Schenau, *A Model of the Human Triceps Surae Muscle-Tendon Complex Applied to Jumping.* *Journal of Biomechanics*, 1986. **19**(11): p. 887-898.
5. Bobbert, M.F., et al., *Biomechanical Analysis of Drop and Countermovement Jumps.* *European Journal of Applied Physiology*, 1986. **54**: p. 566-573.
6. Bobbert, M.F. and A.J.V. Soest, *Effects Of Muscle Strengthening On Vertical Jump Height: A Simulation Study.* *Medicine and Science in Sports and Exercise*, 1994. **26**(8): p. 1012-1020.
7. Brand, R.A., D.R. Pedersen, and J.A. Friedrich, *The Sensitivity of Muscle Force Predictions To Changes In Physiologic Cross-Sectional Area.* *Journal of Biomechanics*, 1986. **19**(8): p. 589-596.
8. Brown, S., et al., *Indicies of Skeletal Muscle Damage and Connective Tissue Breakdown Following Eccentric Muscle Contractions.* *Eur J Appl Physiol*, 1997. **75**: p. 369-374.
9. Cole, G.K., et al., *Modelling of Force Production in Skeletal Muscle Undergoing Stretch.* *Journal of Biomechanics*, 1996. **29**(8): p. 1091-1104.
10. Epstein, M. and W. Herzog, *Hill and Huxley Type Models: Biological Considerations*, in *Theoretical Models of Skeletal Muscle*, J.W. Sons, Editor. 1998, John Wiley & Sons: New York. p. 70-84.
11. Epstein, M. and W. Herzog, *Modeling Skeletal Muscle Using Simple Geometric Shapes: Biological Considerations*, in *Theoretical Models of Skeletal Muscle*, J.W. Sons, Editor. 1998, John Wiley & Sons: New York. p. 23-64.

12. Friden, J., M. Ssjostrom, and B. Ekblom, *Myofibrillar Damage Following Intense Eccentric Exercise in Man*. Int. J. Sports Med., 1983. 4: p. 170-176.
13. Garrett, W.E., *Muscle Strain Injuries: Clinical and Basic Aspects*. Medicine and Science in Sports and Exercise, 1990. 22(4): p. 436-443.
14. Goddard, M.P., et al., *Effects of Accentuated Eccentric Resistance Training and Detraining on Concentric Knee Extensor Strength*. Journal of Strength and Conditioning Research, 1998. 12(1): p. 26-29.
15. Grieve, D.W., S. Pheasant, and P.R. Cavanagh. *Prediction of Gastrocnemius Length From Knee and Ankle Joint Posture*. in *Biomechanics VI-A*. 1978. Baltimore: University Park Press.
16. Hamill, J., G.E. Caldwell, and T.R. Derrick, *Using Shannon's Sampling Theorem*. Journal of Applied Biomechanics, 1997. 13: p. 226-238.
17. Hanavan, E.P., *A Mathematical Model Of The Human Body*. 1964, Aerospace Medical Research Laboratories Wright-Patterson Air Force Base: Ohio. p. 1-73.
18. Herzog, W., *Muscle*, in *Biomechanics of the Musculo-Skeletal System*, B.M.N.a.W. Herzog, Editor. 1994, John Wiley & Sons: New York. p. 154-187.
19. Herzog, W., S. Kamal, and H.D. Clarke, *Myofilament Lengths of Cat Skeletal Muscle: Theoretical Considerations and Functional Implications*. Journal of Biomechanics, 1992. 25(8): p. 945-948.
20. Herzog, W. and L.J. Read, *Lines of Action and Moment Arms of the Major Force-Carrying Structures Crossing the Human Knee Joint*. Journal of Anatomy, 1993. 182: p. 213-230.
21. Hill, A.V., *The Heat of Shortening and the Dynamic Constants of Muscle*. Royal Society of London Proceedings, 1938. 126B: p. 136-195.
22. Housh, D., et al., *Effects of Eccentric-Only Resistance Training and Detraining*. Int. J. Sports Med., 1996. 17: p. 145-148.
23. Jackson, K.M., *Fitting Of Mathematical Functions To Biomechanical Data*. IEEE Transactions In Biomedical Engineering, 1979. 26: p. 122-124.
24. Leger, A.B. and T.E. Milner, *Motor Impairment in the Human Hand Following Eccentric Exercise*. Eur J Appl Physiol, 2001. 84: p. 213-220.

25. Leger, A.B. and T.E. Milner, *Passive and Active Wrist Joint Stiffness Following Eccentric Exercise*. Eur J Appl Physiol, 2000. **82**: p. 472-479.
26. Meijer, K., et al., *A Hill Type Model Of Rat Medial Gastrocnemius Muscle That Accounts For Shotening History Effects*. Journal of Biomechanics, 1998. **31**: p. 555-563.
27. Newham, D., D. Jones, and P. Clarkson, *Repeated High-Force Eccentric Exercise: Effects on Muscle Pain and Damage*. J Appl Physiol, 1987. **63**: p. 1381-1386.
28. Nussbaum, M.A., D.B. Chaffin, and C.J. Rechten, *Muscle Lines-Of-Action Affect Predicted Forces In Optimazation-Based Spine Muscle Modeling*. Journal of Biomechanics, 1995. **28**(4): p. 401-409.
29. Pandy, M.G., et al., *An Optimal Control Model For Maximum-Height Human Jumping*. Journal of Bicrnechanics, 1990. **23**(12): p. 1185-1198.
30. Self, B.P. and D. Paine, *Ankle Biomechanics During Four Landing Techniques*. Medicine and Science in Sports and Exercise, 2001. **33**(8): p. 1338-1344.
31. Soest, A.J.V. and M.F. Bobbert, *The Contribution of Muscle Properties In The Control of Explosive Movements*. Biological Cybernetics, 1993. **69**: p. 195-204.
32. Soest, A.J.V., M.F. Bobbert, and G.J.V.I. Schenau, *A Control Strategy for the Execution of Explosive Movements From Varying Starting Positions*. Journal of Neurophysiology, 1994. **71**(4): p. 1390-1402.
33. Soest, A.J.V., et al., *The Influence of the Biarticularity Of The Gastrocnemius Muscle On Vertical-Jumping Achievement*. Journal of Biomechanics, 1993. **26**(1): p. 1-8.
34. Spoor, C.W., *Balancing A Force On The Fingertip Of A Two-Dimensional Finger Model Without Intrinsic Muscles*, in *Mechanical Models Of Selected Parts Of The Human Musculoskeletal System*, C.W. Spoor, Editor. 1992: Leiden. p. 25-35.
35. Spoor, C.W., et al., *Estimation of Instantaneous Moment Arms Of Lower-Leg Muscles*. Journal of Biomechanics, 1990. **23**(12): p. 1247-1259.
36. Stauber, W.T., *Eccentric Action of Muscles: Physiology, Injury, and Adaptation*, in *Exercise and Sport Sciences Reviews*, P.D. Kent B Pandolf, Editor. 1989, Williams & Wilkins: Baltimore. p. 157-184.

37. Takekura, H., et al., *Eccentric Exercise-Induced Morphological Changes In The Membrane Systems Involved In Excitation-Contraction Coupling In Rat Skeletal Muscle*. *Journal of Physiology*, 2001. **533**(2): p. 571-583.
38. Visser, J.J., et al., *Length and Moment Arm of Human Leg Muscles as a Function of Knee and Hip-Joint Angles*. *Eur J Appl Physiol*, 1990. **61**: p. 453-460.
39. Winter, D.A., *Kinetics: Forces and Moments of Force*, in *Biomechanics And Motor Control of Human Movement*, D.A. Winter, Editor. 1990, John Wiley & Sons: New York. p. 75-102.
40. Winters, J.M., *Hill-Based Muscle Models: A Systems Engineering Perspective*, in *Multiple Muscle Systems*, J.M. Winters and S.L.-Y. Woo, Editors. 1990, Springer-Verlag: New York. p. 69-93.
41. Woittiez, R.D., R.H. Rozendal, and P.A. Huijing. *The Functional Significance of Architecture of the Human Triceps Surae Muscle*. in *Biomechanics IX, International Series on Biomechanics*. 1985: Human Kinetic Publishers.
42. Zahalak, G.I., *A Comparison Of The Mechanical Behavior Of The Cat Soleus Muscle With A Distribution-Moment Model*. *Journal of Biomechanical Engineering*, 1986. **108**: p. 131-140.
43. Zahalak, G.I., *Modeling Muscle Mechanics (and Energetics)*, in *Multiple Muscle Systems Biomechanics and Movement Organization*, J.M. Winters and S.L.-Y. Woo, Editors. 1990, Springer-Verlag: New York. p. 1-23.
44. Zahalak, G.I. and S.-P. Ma, *Muscle Activation and Contraction: Constitutive Relations Based Directly on Cross-Bridge Kinetics*. *Journal of Biomechanical Engineering*, 1990. **112**: p. 52-62.
45. Zhang, S.-N., B.T. Bates, and J.S. Dufek, *Contributions of Lower Extremity Joints to Energy Dissipation During Landings*. *Medicine and Science in Sports and Exercise*, 2000. **32**(4): p. 812-819.

APPENDICES

APPENDIX A

BOBBERT ET AL. EQUATIONS

Equations From Bobbert et al. [4]

$$V_{fibers} = \frac{b[(F_o)_{L_{fibers}} + a]}{(F + a)} - b \quad (1)$$

$$(F_o)_{L_{fibers}} = \left[c_1 \left(\frac{L_{fibers}}{L_{o, fibers}} \right)^2 + c_2 \left(\frac{L_{fibers}}{L_{o, fibers}} \right) + c_3 \right] F_o \quad (2)$$

$$F = \frac{\left[c_1 \left(\frac{L_{fibers}}{L_{o, fibers}} \right)^2 + c_2 \left(\frac{L_{fibers}}{L_{o, fibers}} \right) + c_3 \right] (F_o + a)b}{V_{fibers} + b} - a \quad (3)$$

$$F = c(L_{OI} - L_{fibers} - L_{O, tendon})^2 \quad (4)$$

$$\frac{dF}{dt} = 2c(L_{OI} - L_{fibers} - L_{O, tendon})(V_{OI} - V_{fibers}) \quad (5)$$

$$\frac{dF}{dt} = 2c(L_{OI} - L_{fibers} - L_{O, tendon}) \left[V_{OI} - \left(\frac{b[(F_o)_{L_{fibers}} + a]}{(F + a)} - b \right) \right] \quad (6)$$

Where:

L_{OI}	distance between origin and insertion
L_{fibers}	length of muscle fibers
$L_{o, fibers}$	optimum length of muscle fibers
L_{tendon}	length of tendon
$L_{o, tendon}$	length of tendon when exerted force is zero
V_{OI}	velocity with which origin approaches insertion
V_{fibers}	shortening velocity of muscle fibers
F	exerted force
F_o	isometric force at fiber optimum length
$(F_o)_{L_{fibers}}$	isometric force at some fiber length (L_{fibers}) different from optimum
c	constant
a	the physiological constant in Hill's equation that is proportional to muscle cross-sectional area
b	the physiological constant in Hill's equation that is proportional to muscle fiber optimum length
c_1	-6.25
c_2	12.5
c_3	-5.25

APPENDIX B
PANDY ET AL. EQUATIONS

The equations for body segment dynamics, excitation-contraction dynamics, and equations for the overall musculotendinoskeletal system as given by Pandy et al. [29].

Body-Segmental Dynamics

$$A(\theta)\ddot{\theta} = B(\theta)\dot{\theta}^2 + C(\theta) + DM(\theta)P^T + T(\theta, \dot{\theta})$$

where $\theta, \dot{\theta}, \ddot{\theta}$ are vectors of limb angular displacement, velocity and acceleration; $T(\theta, \dot{\theta})$ is a (4x1) vector of externally applied joint torques; P^T is an (8x1) vector of musculotendon actuator forces; $M(\theta)$ is a (3x8) moment arm matrix formed by computing the perpendicular distance between each musculotendon actuator and the joint it spans; $A(\theta)$ is the (4x4) system mass matrix; $C(\theta)$ is a (4x1) vector containing only gravitational terms; $B(\theta)\dot{\theta}^2$ is a (4x1) vector describing both Coriolis and centrifugal effects, where $\dot{\theta}^2$ represents $\dot{\theta}_i^2$ for $i = 1, 4$; and D is a (4x3) matrix which transforms joint torques into segmental torques.

Excitation-Contraction Dynamics

$$\dot{a}(t) = (1/\tau_{rise})(1-a)u(t) + (1/\tau_{fall})(a_{min} - a)[1-u(t)] \quad u(t) = 0,1$$

where $u(t)$ is the muscle excitation and $[a(t)]$ is the muscle activation

Musculotendinoskeletal System Dynamic Equations

$$\ddot{\theta} = A(\theta)^{-1} [B(\theta)\dot{\theta}^2 + C(\theta) + DM(\theta)P^T + T(\theta, \dot{\theta})]$$

$$\dot{P}_i^T = f(\theta, \dot{\theta}, P_i^T, a_i) \quad i = 1,8$$

$$\dot{a}_i(t) = (1/\tau_{rise})(1-a)u_i + (1/\tau_{fall})(a_{min} - a_i)[1-u_i] \quad i = 1,8$$

where the state vector defined by $[x_1, x_2, x_3, x_4]^T = [\theta, \dot{\theta}, P^T, a]^T$ is composed of 24 elements: four angular displacements $\theta_i, i=1,4$, four angular velocities $\dot{\theta}_i, i=1,4$, eight muscle activations $a_i, i=1,8$ and eight musculotendon actuator forces $P_i^T, i=1,8$.

APPENDIX C

GRIEVE ET AL. COEFFICIENTS

Table 1. Coefficients for predicting change in muscle length as described by Grieve et al. [15].

	A_0	A_1	A_2
Ankle	-22.18468	0.30141	-0.00061
Knee	6.46251	-0.07987	0.00011

APPENDIX D

ANTHROPOMETRIC MEASUREMENTS AND DEFINITIONS

Table 2. Anthropometric measurements and definitions.

Anthropometric Measurement

FDC=	Foot Distal Circumference
FPH=	Height of Lateral Malleolus
FL=	Foot Length
LDC=	Leg Distal Circumference
LPC=	Leg Proximal Circumference
LL=	Leg Length
TDC=	Thigh Distal Circumference
TPC=	Thigh Proximal Circumference
TL=	Thigh Length
AMA=	Ankle Moment Arm

Measurement Definition

FDC=	Circumferential measurement from head of first metatarsal to the fifth metatarsal
FPH=	Height measurement from floor to center of the lateral malleolus
FL=	Length measurement from the lateral malleolus to the head of the fifth metatarsal marker
LDC=	Circumferential measurement of the ankle superior to the malleolus
LPC=	Circumferential measurement of widest girth of the leg
LL=	Length of measurement from the ankle to the tibial epicondyle marker
TDC=	Circumferential measurement of femur just superior to the femoral epicondyle
TPC=	Circumferential measurement of the widest girth of the thigh
TL=	Length measurement from the tibial epicondyle marker to the hip marker
AMA=	Length measurement from center of the heel marker to midline of the Achilles' Tendon

APPENDIX E
LOWER LEG AND FOOT SYMBOLS AND EQUATIONS

Symbols and equations representing the dimensions and properties of the lower leg and foot.

Lower Leg

$$R = \frac{GKNEC}{2\pi}$$

$$RR = \frac{ANKC}{2\pi}$$

$$SL = TIBH - SPHYH$$

$$SW = .5BLL$$

$$SM = SW + 32.2$$

Foot

$$R = .5SPHYH$$

$$SL = FOOTL$$

$$ETA = .429$$

$$SW = 0.5BF$$

$$SM = SW + 32.2$$

Where:

- R radius of segment
- RR radius small radius of segment
- SL segment length
- SW segment weight
- SM segment mass

APPENDIX F
ECCENTRIC MUSCLE FORCE EQUATIONS

Equations and variables describing the calculation of the eccentric force generated by the calf muscle.

$$c_1 = \frac{B_{REL} \cdot F_{LEN}^2 (1 - F_{ASYMP})^2}{SF(F_{LEN} + A_{REL})}$$

$$c_2 = -F_{LEN} F_{ASYMP}$$

$$c_3 = \frac{B_{REL} \cdot F_{LEN} (1 - F_{ASYMP})}{SF(F_{LEN} + A_{REL})}$$

A_{REL} , and B_{REL}	describe the shape of the hyperbolic relation and are 0.23 and 1.28
SF	describes the discontinuity in the force-velocity curve at zero velocity and is 2.0
F_{ASYMP}	asymptotic value of the force and is 1.5
SL	modifies force-velocity relation at high velocities of stretch (300)
$L_{CE(OPT)}$	optimal contractile element length and is 0.03257 m
F_{MAX}	maximal isometric force at optimal length 1.0
F_{LEN}	relative isometric force; ratio of the isometric force at a given length to the maximal isometric force

APPENDIX G
SUBJECT INFORMATION

Table 3. Subject Information

Subject	Age	Weight (kg)	Height (cm)
1	30	61.33	165.00
2	26	72.93	175.26
3	26	72.52	185.42
4	20	83.81	180.34
5	19	70.38	177.80
6	21	76.82	187.96
7	26	75.21	170.18
8	23	66.08	180.34
9	24	86.22	187.96
10	19	75.08	187.96
Mean	23.4	74.0	179.82
Standard Deviation	3.66	7.42	7.95

APPENDIX H
VERTICAL GROUND REACTION FORCE DATA

Table 6. Condition means and standard deviations of VGRF.

Cond	F1	F2	LrateF1	LrateF2	Imp	MaxBrF	TmaxBrF	MProp	TMaxProp
1 (NL)	32.44 (2.13)	57.39 (4.85)	2980.20 (140.79)	1478.63 (265.83)	2.91 (0.17)	-14.04 (0.85)	0.011 (0.0)	16.47 (2.25)	0.051 (0.007)
2 (SL)	39.31 (1.84)	77.65 ^a (3.72)	3469.85 (385.55)	2093.18 (403.88)	3.71 ^a (0.08)	-15.58 (0.77)	0.012 (0.003)	20.04 (3.22)	0.050 (0.005)
3 (SF)	-- --	104.80 ^{a,b} (7.75)	-- --	5188.54 ^{a,b} (1461.43)	3.67 ^a (0.11)	-18.96 (4.16)	0.012 (0.004)	21.95 (3.14)	0.042 (0.009)
4 (SC)	-- --	47.30 ^{b,c} (3.08)	-- --	865.26 ^c (83.72)	3.45 (0.19)	10.71 ^{a,b,c} (0.78)	0.013 (0.002)	8.46 ^{a,b,c} (1.18)	0.035 ^{a,b,c} (0.010)

Note: Force unit is in N/kg and time unit is in seconds.

Loading rate unit is in N/kg/s.

Impulse unit is in (N/kg)*s.

Maximum breaking force unit is in N/kg

Maximum propulsion force unit is in N/kg.

Standard deviation values are in parenthesis.

The definitions of variables are in Appendix A.

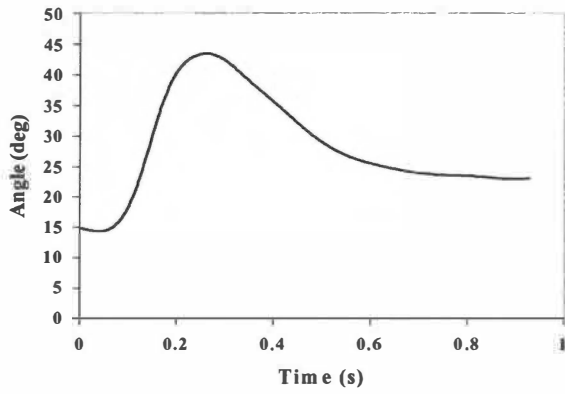
^a denotes significant difference from the normal landing (NL) condition 1.

^b denotes significant difference from the stiff landing with minimal knee flexion (SL) condition 2.

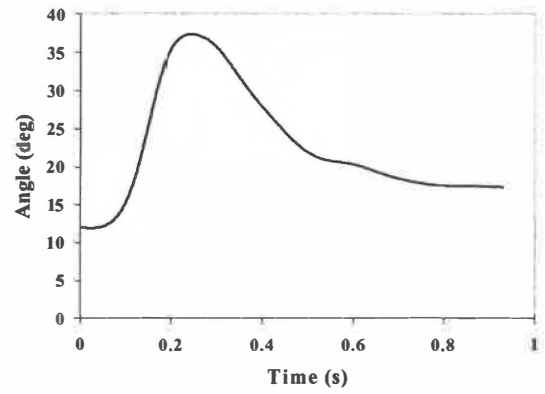
^c denotes significant difference from the stiff landing but landing flat footed (SF) condition 3.

SC is a stiff landing but landing only on the forefoot and contracting the calf muscle.

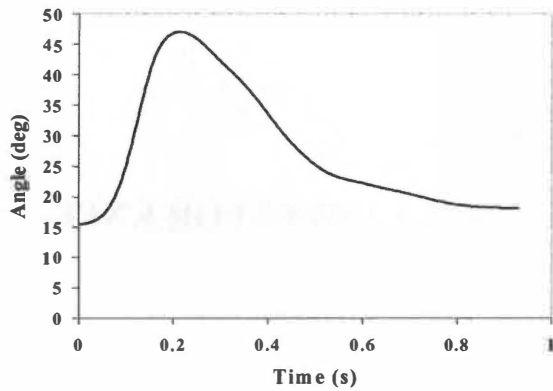
APPENDIX I
REPRESENTATIVE JOINT ANGLE CURVES FOR HIP



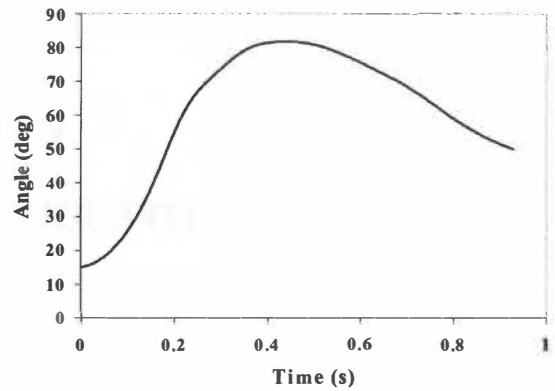
(a)



(b)



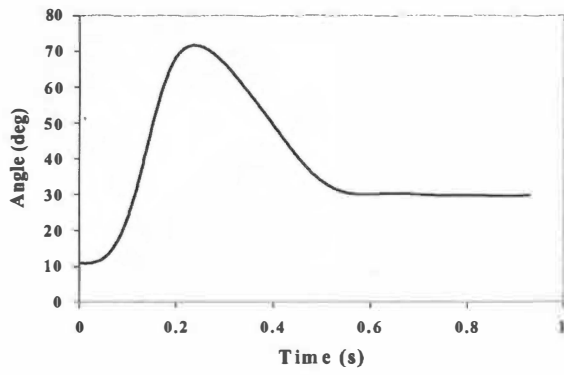
(c)



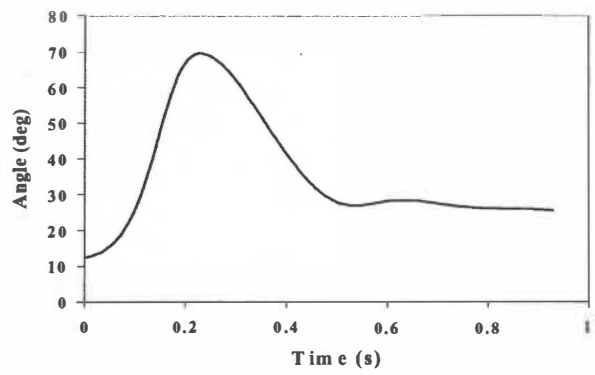
(d)

Figure 5. Representative curves for hip joint angle for (a) normal landing (NL), (b) stiff landing with minimal knee flexion (SL), (c) stiff landing but landing flat footed (SF), and (d) stiff landing but landing only on the toes and contracting the calf muscle (SC).

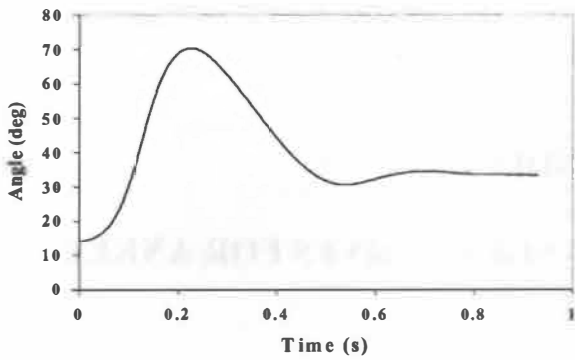
APPENDIX J
REPRESENTATIVE JOINT ANGLE CURVES FOR KNEE



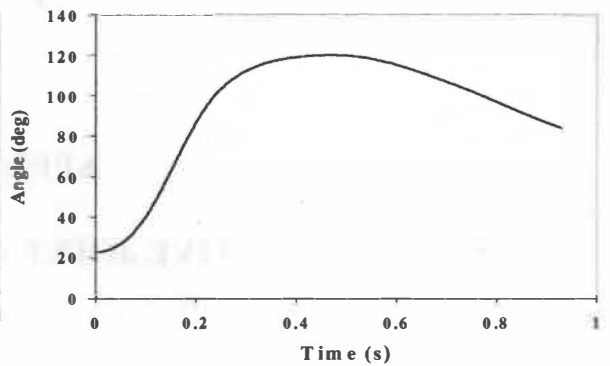
(a)



(b)



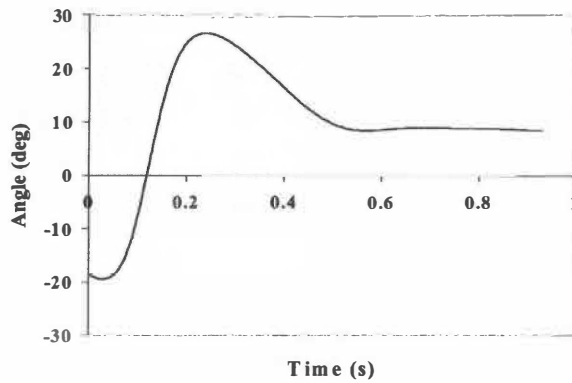
(c)



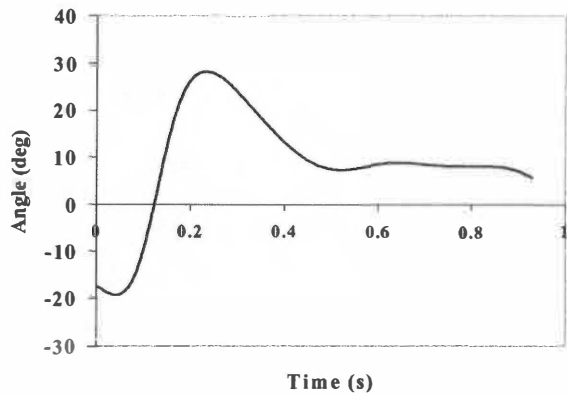
(d)

Figure 6. Representative curves for knee angle joint for (a) normal landing (NL), (b) stiff landing with minimal knee flexion (SL), (c) stiff landing but landing flat footed (SF), and (d) stiff landing but landing only on the toes and contracting the calf muscle (SC).

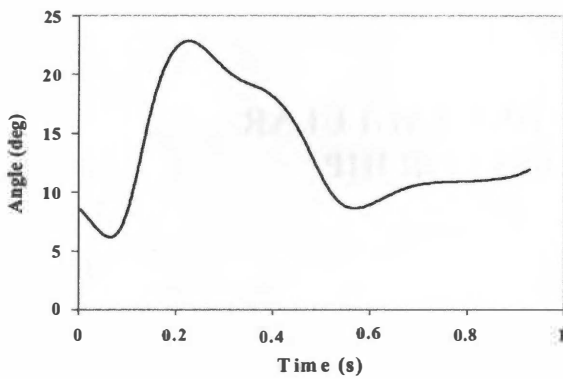
APPENDIX K
REPRESENTATIVE JOINT ANGLE CURVES FOR ANKLE



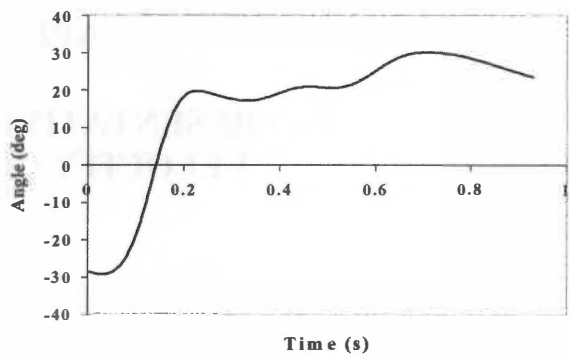
(a)



(b)



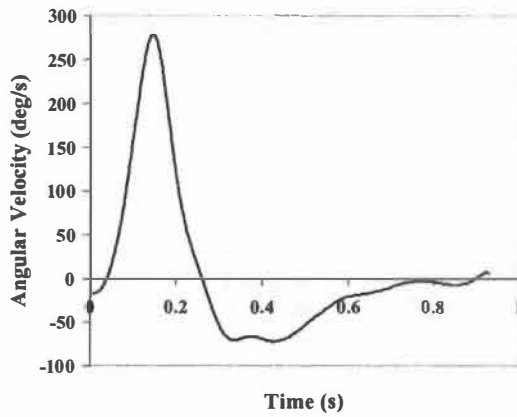
(c)



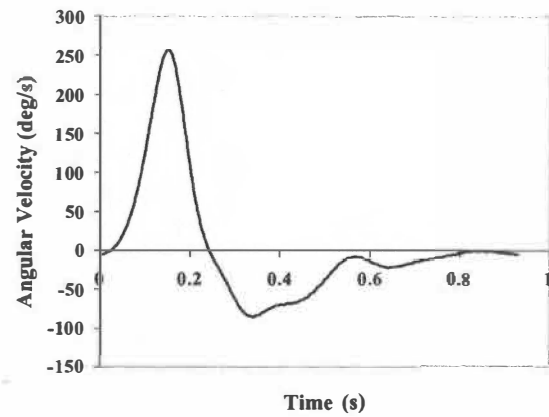
(d)

Figure 7. Representative curves for ankle joint angle for (a) normal landing (NL), (b) stiff landing with minimal knee flexion (SL), (c) stiff landing but landing flat footed (SF), and (d) stiff landing but landing only on the toes and contracting the calf muscle (SC).

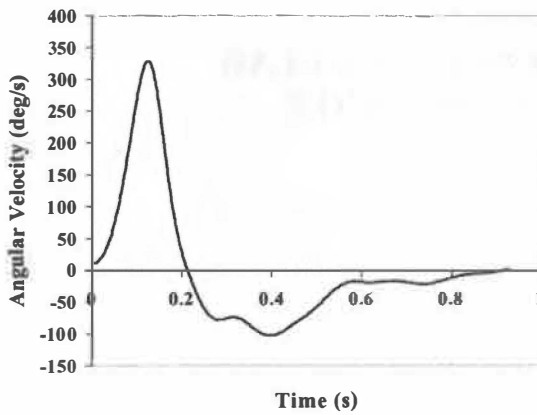
APPENDIX L
REPRESENTATIVE JOINT ANGLULAR
VELOCITY CURVES FOR HIP



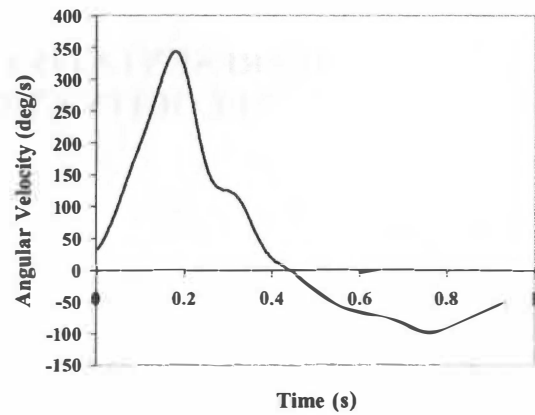
(a)



(b)



(c)

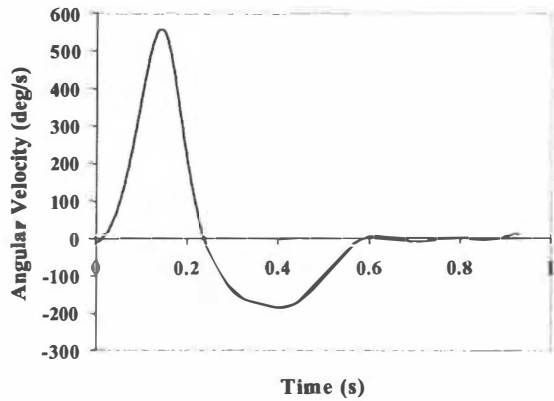


(d)

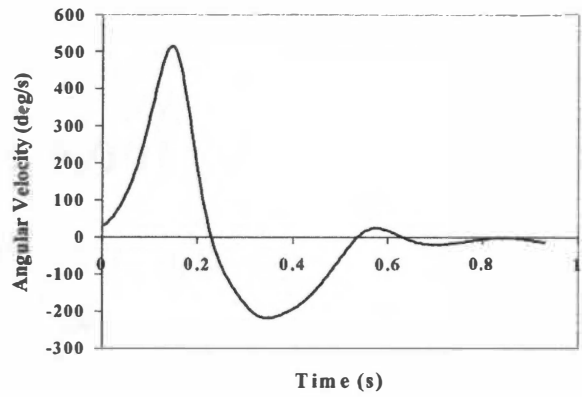
Figure 8. Representative curves for hip joint angular velocity for (a) normal landing (NL), (b) stiff landing with minimal knee flexion (SL), (c) stiff landing but landing flat footed (SF), and (d) stiff landing but landing only on the toes and contracting the calf muscle (SC).

APPENDIX M

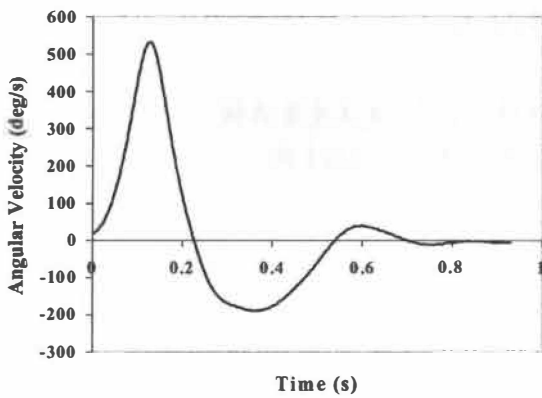
**REPRESENTATIVE JOINT ANGLULAR
VELOCITY CURVES FOR KNEE**



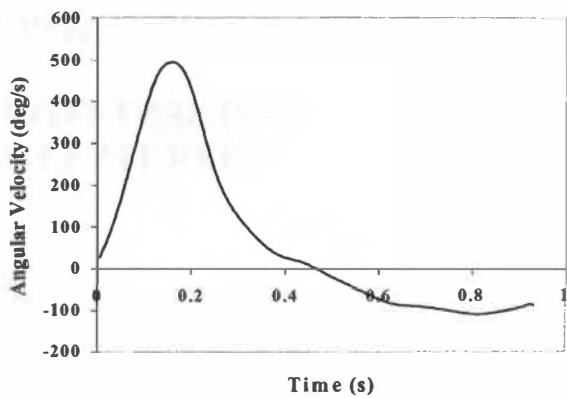
(a)



(b)



(c)

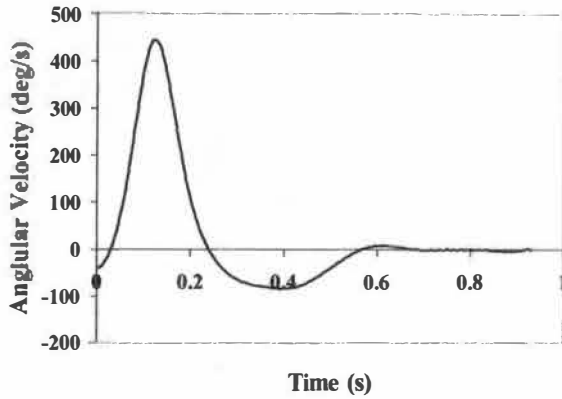


(d)

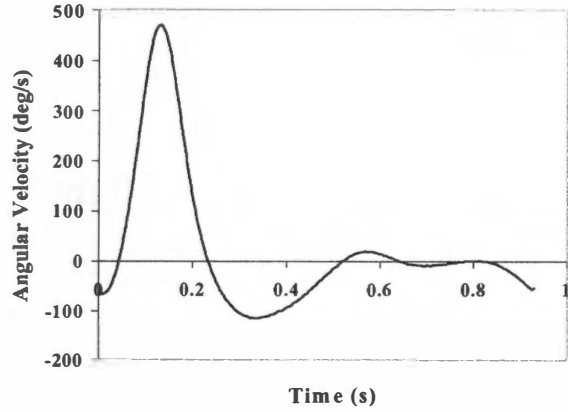
Figure 9. Representative curve for knee joint angular velocity for (a) normal landing (NL), (b) stiff landing with minimal knee flexion (SL), (c) stiff landing but landing flat footed (SF), and (d) stiff landing but landing only on the toes and contracting the calf muscle (SC).

APPENDIX N

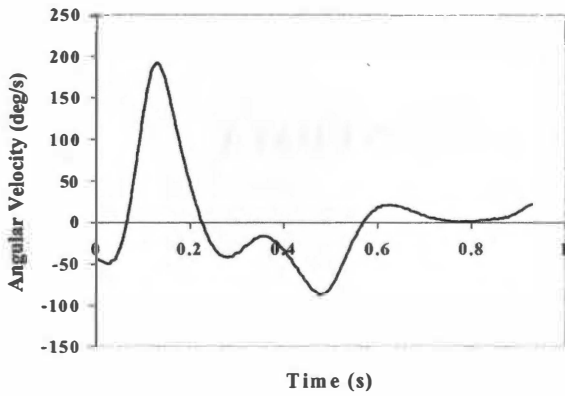
**REPRESENTATIVE JOINT ANGLULAR
VELOCITY CURVES FOR ANKLE**



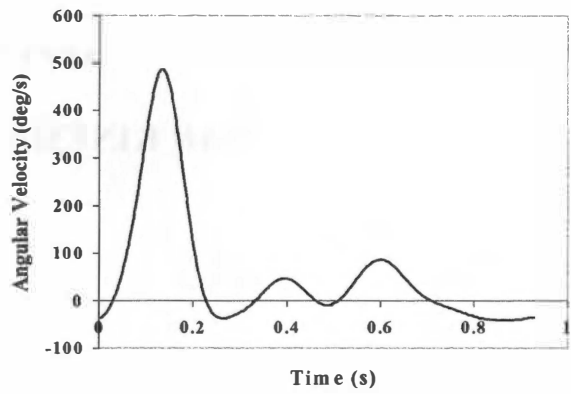
(a)



(b)



(c)



(d)

Figure 10. Representative curves for ankle joint angular velocity for (a) normal landing (NL), (b) stiff landing with minimal knee flexion (SL), (c) stiff landing but landing flat footed (SF), and (d) stiff landing but landing only on the toes and contracting the calf muscle (SC).

APPENDIX O
ANGULAR KINEMATIC HIP JOINT DATA

Table 7. Condition means and standard deviations of angular kinematic hip joint variables.

Cond	Cont	Max	Tmax	Min	Tmin	ROM	ContVel	MaxVel	TmaxVel
1 (NL)	23.45 (0.78)	70.94 (2.15)	0.316 (0.086)	16.78 (22.15)	0.380 (0.197)	47.49 (1.87)	180.61 (14.33)	311.76 (13.97)	0.075 (0.095)
2 (SL)	18.58 ^a (1.36)	38.96 ^a (3.53)	0.159 ^a (0.021)	15.10 (1.52)	0.413 (0.167)	20.38 ^a (2.86)	127.89 ^a (15.91)	210.21 ^a (17.59)	0.047 (0.009)
3 (SF)	20.83 (1.65)	44.61 (3.12)	0.175 ^a (0.025)	15.69 (1.34)	0.432 (0.171)	23.79 ^a (2.03)	186.61 ^b (30.60)	265.40 (16.60)	0.037 (0.012)
4 (SC)	19.48 (0.69)	49.52 ^a (23.24)	0.254 (0.134)	15.47 (1.61)	0.354 (0.175)	30.03 (24.13)	114.57 ^{a,c} (7.10)	221.33 (138.78)	0.092 (0.131)

Note: Angle and ROM units are in degrees and time unit is in s.
Velocity unit is in deg/s.

Standard deviation values are in parenthesis.

The definitions of variables are in Appendix A.

^a denotes significant difference from the normal landing (NL) condition 1.

^b denotes significant difference from the stiff landing with minimal knee flexion (SL) condition 2.

^c denotes significant difference from the stiff landing but landing flat footed (SF) condition 3.

SC is a stiff landing but landing only on the forefoot and contracting the calf muscle.

APPENDIX P

ANGULAR KINEMATIC KNEE JOINT DATA

Table 8. Condition means and standard deviations of angular kinematic knee joint variables.

Cond	Cont	Max	Tmax	Min	Tmin	ROM	ContVel	MaxVel	TmaxVel
1 (NL)	33.33 (0.87)	93.12 (2.54)	0.245 (0.035)	26.00 (1.50)	0.477 (0.185)	59.78 (1.45)	321.85 (21.41)	493.26 (8.67)	0.052 (0.005)
2 (SL)	26.58 ^a (1.25)	67.24 ^a (2.07)	0.141 ^a (0.013)	21.71 (1.34)	0.429 (0.168)	40.66 ^a (2.22)	288.05 (24.54)	440.28 ^a (24.49)	0.048 (0.011)
3 (SF)	30.15 (1.90)	69.15 ^a (1.96)	0.131 ^a (0.011)	22.46 (2.96)	0.435 (0.160)	38.10 ^a (1.43)	349.28 ^b (29.62)	490.02 ^b (12.51)	0.037 ^{a,b} (0.011)
4 (SC)	30.42 (0.90)	75.78 ^a (19.88)	0.194 (0.111)	25.19 (1.80)	0.336 (0.166)	45.36 (20.19)	276.46 (15.33)	400.31 ^c (82.85)	0.053 (0.022)

Note: Angle and ROM units are in degrees and time unit is in s.

Velocity unit is in deg/s.

Standard deviation values are in parenthesis.

The definitions of variables are in Appendix A.

^a denotes significant difference from the normal landing (NL) condition 1.

^b denotes significant difference from the stiff landing with minimal knee flexion (SL) condition 2.

^c denotes significant difference from the stiff landing but landing flat footed (SF) condition 3.

SC is a stiff landing but landing only on the forefoot and contracting the calf muscle.

APPENDIX Q

ANGULAR KINEMATIC ANKLE JOINT DATA

Table 9. Condition means and standard deviations of angular kinematic ankle joint variables.

Cond	Cont	Max	Tmax	Min	Tmin	ROM	ContVel	MaxVel	TmaxVel
1 (NL)	-11.97 (2.67)	29.93 (4.90)	0.207 (0.087)	-12.24 (2.05)	0.046 (0.161)	41.90 (4.73)	404.69 (22.82)	506.59 (28.52)	0.040 (0.097)
2 (SL)	-14.32 (2.93)	23.52 ^a (0.94)	0.143 (0.025)	-14.32 (2.93)	0.000 (0.0)	37.85 (3.04)	392.99 (33.85)	493.78 (38.62)	0.026 (0.010)
3 (SF)	1.05 ^{a,b} (3.53)	23.81 (1.10)	0.120 ^{a,b} (0.014)	-2.20 ^{a,b} (2.08)	0.234 (0.151)	22.76 ^{a,b} (3.18)	238.56 ^{a,b} (37.88)	309.94 ^{a,b} (45.74)	0.050 (0.119)
4 (SC)	-20.61 ^c (1.69)	17.67 ^a (2.50)	0.191 (0.136)	-21.96 ^{a,b,c} (1.68)	0.040 (0.064)	38.28 ^c (2.76)	434.32 ^c (34.73)	529.24 ^c (24.82)	0.025 (0.004)

Note: Angle and ROM units are in degrees and time unit is in s.

Velocity unit is in deg/s.

Standard deviation values are in parenthesis.

The definitions of variables are in Appendix A.

^a denotes significant difference from the normal landing (NL) condition 1.

^b denotes significant difference from the stiff landing with minimal knee flexion (SL) condition 2.

^c denotes significant difference from the stiff landing but landing flat footed (SF) condition 3.

SC is a stiff landing but landing only on the forefoot and contracting the calf muscle.

APPENDIX R
SUBJECT ANGULAR KINEMATIC HIP JOINT DATA

Table 10. Subject means and standard deviations of angular kinematic hip joint variables.

Subj	Cond						Cont			
		Cont	Max	Tmax	Min	Tmin	ROM	Vel	MaxVel	Tmax Vel
1	1	37.53 (3.74)	100.91 (5.51)	0.485 (0.129)	37.53 (3.74)	0.000 (0.0)	63.38 (8.74)	175.63 (10.53)	355.46 (34.44)	0.062 (0.005)
	2	34.74 (3.59)	62.60 (13.56)	0.202 (0.073)	31.06 (6.74)	0.423 (0.413)	27.86 (11.19)	136.00 (6.18)	260.47 (56.84)	0.050 (0.010)
	3	28.82 (3.08)	53.45 (5.12)	0.195 (0.015)	27.81 (1.40)	0.138 (0.309)	24.63 (4.59)	100.24 (44.10)	265.72 (28.91)	0.054 (0.012)
	4	33.69 (1.95)	69.56 (7.24)	0.254 (0.049)	29.96 (2.88)	0.413 (0.452)	35.87 (7.11)	110.81 (17.91)	268.52 (19.92)	0.073 (0.010)
2	1	15.89 (1.96)	82.14 (3.84)	0.330 (0.025)	8.96 (15.22)	0.165 (0.369)	66.25 (4.94)	230.94 (38.21)	398.20 (18.24)	0.053 (0.010)
	2	11.51 (4.76)	41.82 (7.30)	0.228 (0.049)	11.51 (4.76)	0.000 (0.0)	30.31 (5.43)	186.71 (46.53)	313.43 (40.05)	0.046 (0.007)
	3	10.53 (4.36)	55.64 (8.07)	0.312 (0.037)	10.53 (4.36)	0.000 (0.0)	45.12 (7.41)	233.52 (50.48)	333.82 (42.74)	0.042 (0.008)
	4	9.84 (2.63)	87.12 (78.12)	0.427 (0.246)	9.84 (2.63)	0.000 (0.0)	77.28 (80.35)	124.52 (11.40)	507.14 (461.76)	0.108 (0.077)
3	1	18.77 (1.73)	38.43 (4.85)	0.183 (0.045)	-16.07 (73.55)	0.613 (0.357)	19.66 (5.12)	120.98 (16.95)	175.46 (33.76)	0.061 (0.023)
	2	14.85 (0.94)	23.25 (3.73)	0.112 (0.015)	10.44 (3.08)	0.565 (0.258)	8.40 (2.82)	74.73 (10.91)	96.33 (27.14)	0.038 (0.017)
	3	26.04 (3.45)	52.29 (6.71)	0.157 (0.016)	9.36 (8.85)	0.819 (0.013)	26.25 (3.91)	271.16 (57.55)	522.67 (479.92)	0.184 (0.358)
	4	11.70 (1.83)	35.63 (22.68)	0.416 (0.374)	6.27 (3.98)	0.335 (0.264)	23.93 (23.50)	53.26 (27.52)	124.52 (64.07)	0.238 (0.304)
4	1	16.04 (2.52)	42.10 (3.01)	0.295 (0.297)	8.97 (4.57)	0.761 (0.125)	26.06 (2.93)	109.65 (45.14)	253.42 (30.43)	0.209 (0.310)
	2	10.49 (2.52)	32.57 (2.93)	0.134 (0.009)	9.86 (1.95)	0.330 (0.452)	22.08 (4.29)	127.98 (22.23)	238.21 (40.66)	0.062 (0.012)
	3	18.79 (5.71)	47.90 (3.92)	0.192 (0.084)	14.68 (2.37)	0.462 (0.427)	29.11 (4.19)	239.01 (76.04)	346.98 (60.35)	0.039 (0.015)
	4	16.08 (2.54)	32.23 (6.08)	0.139 (0.013)	13.28 (3.86)	0.449 (0.413)	16.15 (4.16)	116.29 (29.04)	165.35 (33.76)	0.213 (0.338)
5	1	21.44 (3.40)	71.14 (3.34)	0.287 (0.026)	19.03 (2.10)	0.330 (0.452)	49.69 (6.48)	174.33 (32.78)	344.34 (12.61)	0.064 (0.011)
	2	12.84 (1.72)	21.86 (6.67)	0.084 (0.027)	3.44 (3.09)	0.609 (0.242)	9.02 (5.87)	88.80 (32.34)	133.10 (69.29)	0.031 (0.018)
	3	10.57 (1.06)	21.01 (3.72)	0.089 (0.016)	1.65 (2.40)	0.538 (0.236)	10.44 (3.60)	83.61 (8.60)	162.15 (38.52)	0.041 (0.011)
	4	10.26 (1.34)	11.06 (1.59)	0.038 (0.009)	-4.35 (3.21)	0.745 (0.161)	0.81 (0.40)	32.57 (10.11)	32.57 (10.11)	0.000 (0.0)

Table 10. (Continued).

Subj	Cond	Cont	Max	Tmax	Min	Tmin	ROM	ContVel	MaxVel	TmaxVel
6	1	31.74 (4.30)	81.35 (8.15)	0.274 (0.020)	27.64 (2.97)	0.660 (0.369)	49.61 (7.97)	245.32 (51.45)	330.37 (42.24)	0.048 (0.018)
	2	27.49 (3.14)	60.02 (7.92)	0.229 (0.021)	23.29 (4.48)	0.655 (0.366)	32.53 (7.07)	183.66 (39.06)	260.72 (43.14)	0.042 (0.010)
	3	30.13 (3.47)	60.76 (9.53)	0.180 (0.018)	28.64 (6.02)	0.165 (0.369)	30.63 (6.34)	305.24 (16.60)	336.84 (23.88)	0.018 (0.005)
	4	22.23 (1.11)	45.09 (3.14)	0.200 (0.022)	19.74 (3.32)	0.660 (0.369)	22.86 (2.08)	133.69 (9.26)	190.61 (13.03)	0.049 (0.005)
7	1	24.14 (3.14)	89.38 (5.98)	0.408 (0.022)	24.14 (3.14)	0.000 (0.0)	65.24 (8.07)	209.00 (7.89)	388.43 (40.38)	0.060 (0.004)
	2	20.67 (3.68)	41.57 (2.85)	0.133 (0.015)	19.89 (3.29)	0.135 (0.302)	20.91 (4.0)	187.69 (31.41)	270.82 (29.82)	0.035 (0.010)
	3	24.10 (2.16)	41.47 (5.01)	0.096 (0.010)	16.78 (4.23)	0.817 (0.010)	17.36 (3.08)	260.53 (22.08)	296.82 (30.11)	0.020 (0.003)
	4	26.30 (1.41)	78.21 (6.10)	0.338 (0.061)	26.30 (1.41)	0.000 (0.0)	51.91 (7.22)	183.92 (15.94)	336.49 (13.58)	0.077 (0.002)
8	1	18.88 (3.32)	58.77 (7.12)	0.312 (0.069)	18.88 (3.32)	0.000 (0.0)	39.90 (5.14)	151.74 (25.50)	257.89 (35.48)	0.056 (0.010)
	2	18.96 (3.22)	48.68 (3.10)	0.248 (0.037)	18.96 (3.22)	0.000 (0.0)	29.72 (1.99)	100.52 (56.98)	244.64 (12.13)	0.074 (0.038)
	3	20.79 (3.15)	49.85 (9.04)	0.247 (0.057)	20.75 (3.21)	0.004 (0.009)	29.07 (7.89)	142.65 (91.70)	273.76 (48.35)	0.059 (0.044)
	4	20.63 (2.97)	49.58 (1.38)	0.268 (0.072)	20.06 (2.58)	0.165 (0.369)	28.95 (3.18)	118.36 (10.65)	212.79 (25.72)	0.068 (0.006)
9	1	22.59 (2.94)	57.52 (9.55)	0.234 (0.028)	14.60 (1.63)	0.775 (0.069)	34.93 (7.08)	170.27 (22.31)	281.86 (54.64)	0.057 (0.007)
	2	17.59 (1.08)	28.10 (1.99)	0.100 (0.010)	12.94 (2.68)	0.657 (0.367)	10.51 (1.34)	96.32 (15.80)	146.66 (14.32)	0.041 (0.010)
	3	22.71 (2.79)	40.78 (4.44)	0.169 (0.064)	13.48 (2.75)	0.803 (0.042)	18.07 (3.01)	198.66 (35.37)	248.44 (11.30)	0.024 (0.009)
	4	20.78 (1.93)	39.14 (7.16)	0.285 (0.302)	14.04 (5.90)	0.467 (0.428)	18.36 (6.52)	114.35 (19.98)	158.43 (17.78)	0.046 (0.006)

Table 10. (Continued).

Subj	Cond	Cont	Max	Tmax	Min	Tmin	ROM	ContVel	MaxVel	TmaxVel
10	1	27.44 (3.28)	87.63 (4.41)	0.349 (0.044)	24.13 (5.61)	0.495 (0.452)	60.19 (4.41)	218.28 (24.91)	332.21 (9.94)	0.078 (0.005)
	2	16.64 (0.81)	29.10 (4.11)	0.123 (0.011)	9.66 (1.48)	0.760 (0.081)	12.46 (3.55)	96.50 (27.81)	137.73 (34.25)	0.051 (0.005)
	3	27.00 (5.64)	52.03 (12.74)	0.161 (0.039)	12.18 (4.41)	0.825 (0.0)	25.03 (7.44)	227.92 (81.78)	293.16 (64.03)	0.032 (0.011)
	4	23.33 (3.04)	47.55 (9.06)	0.178 (0.055)	19.56 (6.82)	0.311 (0.427)	24.22 (6.50)	157.93 (19.77)	216.84 (33.92)	0.052 (0.017)

Note: Angle and ROM units are in degrees and time unit is in seconds.

Velocity unit is in deg/s.

Standard deviation values are in parenthesis.

The definitions of variables are in Appendix H.

APPENDIX S
SUBJECT ANGULAR KINEMATIC KNEE JOINT DATA

Table 11. Subject means and standard deviations of angular kinematic knee joint variables.

Subj	Cond	Cont	Max	Tmax	Min	Tmin	ROM	ContVel	MaxVel	TmaxVel
1	1	35.13 (3.94)	88.73 (1.27)	0.175 (0.012)	35.13 (3.94)	0.000 (0.0)	53.60 (5.01)	336.15 (34.36)	511.07 (29.03)	0.050 (0.007)
	2	33.05 (2.81)	79.88 (4.99)	0.154 (0.017)	30.00 (3.41)	0.492 (0.449)	46.83 (6.95)	280.13 (24.86)	482.70 (52.06)	0.052 (0.008)
	3	25.74 (2.56)	71.07 (3.96)	0.138 (0.012)	24.23 (1.72)	0.255 (0.373)	45.33 (4.29)	233.65 (59.89)	521.58 (21.36)	0.054 (0.010)
	4	36.32 (1.51)	82.89 (3.01)	0.153 (0.008)	35.34 (1.67)	0.206 (0.452)	46.57 (2.39)	291.18 (16.44)	441.47 (23.05)	0.058 (0.003)
2	1	30.37 (2.29)	100.41 (2.69)	0.297 (0.019)	27.47 (5.44)	0.330 (0.452)	70.04 (4.03)	345.55 (45.22)	566.48 (25.20)	0.050 (0.009)
	2	22.14 (3.37)	71.70 (3.04)	0.146 (0.010)	22.14 (3.37)	0.000 (0.0)	49.56 (3.07)	344.80 (53.10)	556.62 (31.80)	0.046 (0.007)
	3	31.93 (2.36)	84.89 (6.46)	0.169 (0.027)	31.93 (2.36)	0.000 (0.0)	52.96 (5.87)	411.29 (26.03)	556.24 (28.01)	0.038 (0.006)
	4	26.60 (0.87)	118.88 (67.03)	0.426 (0.365)	26.60 (0.87)	0.000 (0.0)	92.28 (67.32)	267.16 (14.94)	605.76 (286.27)	0.110 (0.075)
3	1	28.61 (2.66)	78.43 (8.99)	0.200 (0.029)	17.96 (5.07)	0.772 (0.118)	49.82 (7.72)	333.89 (7.19)	390.61 (21.73)	0.046 (0.017)
	2	20.50 (1.80)	51.43 (6.57)	0.122 (0.011)	9.62 (4.66)	0.648 (0.159)	30.92 (5.23)	272.47 (11.39)	332.65 (35.45)	0.041 (0.017)
	3	27.52 (3.51)	56.87 (5.72)	0.118 (0.016)	13.68 (6.79)	0.765 (0.080)	29.35 (2.92)	334.85 (43.56)	408.79 (25.55)	0.026 (0.006)
	4	25.14 (2.13)	54.06 (9.26)	0.132 (0.020)	12.85 (5.03)	0.776 (0.069)	28.92 (7.54)	290.32 (20.20)	325.40 (31.32)	0.024 (0.007)
4	1	25.95 (3.24)	71.74 (4.49)	0.171 (0.024)	20.98 (3.15)	0.818 (0.015)	45.79 (6.67)	141.26 (77.52)	451.68 (38.96)	0.073 (0.018)
	2	20.20 (3.18)	61.77 (2.71)	0.142 (0.010)	20.20 (3.18)	0.000 (0.0)	41.57 (3.81)	229.48 (33.30)	423.15 (25.19)	0.058 (0.006)
	3	26.94 (5.26)	62.00 (2.36)	0.119 (0.020)	22.58 (7.54)	0.253 (0.347)	35.06 (6.41)	306.43 (92.73)	465.20 (55.69)	0.041 (0.015)
	4	28.34 (3.42)	69.51 (4.90)	0.154 (0.021)	28.34 (3.42)	0.000 (0.0)	41.18 (4.45)	260.63 (65.89)	386.16 (20.83)	0.056 (0.025)
5	1	30.63 (3.32)	103.83 (5.01)	0.276 (0.043)	24.58 (3.78)	0.825 (0.0)	73.20 (5.26)	322.32 (53.01)	566.19 (18.99)	0.062 (0.010)
	2	17.19 (2.10)	47.91 (8.68)	0.104 (0.013)	9.53 (1.55)	0.687 (0.199)	30.71 (9.60)	275.57 (38.59)	399.70 (95.76)	0.038 (0.015)
	3	15.88 (2.09)	52.54 (4.45)	0.104 (0.008)	8.52 (0.81)	0.682 (0.219)	36.65 (5.20)	301.18 (31.38)	485.58 (49.26)	0.045 (0.006)
	4	21.49 (2.30)	38.04 (2.70)	0.089 (0.004)	12.50 (2.28)	0.698 (0.227)	16.54 (1.54)	256.55 (25.18)	274.53 (21.49)	0.015 (0.006)

Table 11. (Continued).

Subj	Cond	Cont	Max	Tmax	Min	Tmin	ROM	ContVel	MaxVel	TmaxVel
6	1	43.90 (4.35)	93.11 (5.55)	0.200 (0.010)	24.57 (5.74)	0.825 (0.0)	49.21 (5.39)	363.87 (49.02)	444.88 (31.06)	0.037 (0.013)
	2	41.42 (4.88)	84.31 (7.14)	0.178 (0.026)	33.04 (4.33)	0.660 (0.369)	42.90 (6.35)	290.66 (26.18)	417.49 (38.24)	0.044 (0.004)
	3	44.40 (3.89)	78.82 (6.74)	0.132 (0.018)	38.23 (7.08)	0.650 (0.364)	34.42 (3.44)	385.84 (42.53)	451.20 (20.84)	0.022 (0.005)
	4	37.40 (1.76)	73.64 (2.70)	0.148 (0.005)	27.10 (4.96)	0.798 (0.059)	36.23 (1.41)	258.03 (22.38)	360.49 (23.77)	0.045 (0.002)
7	1	33.02 (4.49)	102.68 (3.33)	0.357 (0.117)	33.02 (4.49)	0.000 (0.0)	69.66 (6.49)	386.62 (11.38)	541.98 (44.49)	0.048 (0.002)
	2	28.97 (5.10)	67.18 (3.18)	0.116 (0.012)	24.59 (4.67)	0.399 (0.293)	38.21 (6.94)	400.02 (32.39)	516.66 (45.59)	0.031 (0.010)
	3	31.63 (1.40)	63.36 (4.06)	0.098 (0.015)	18.30 (9.80)	0.368 (0.049)	31.73 (4.09)	436.68 (40.87)	509.89 (40.29)	0.023 (0.004)
	4	26.30 (1.41)	78.21 (6.10)	0.338 (0.061)	26.30 (1.41)	0.000 (0.0)	51.91 (7.22)	183.92 (15.94)	336.49 (13.58)	0.077 (0.002)
8	1	31.63 (3.43)	95.92 (4.09)	0.282 (0.045)	31.63 (3.43)	0.000 (0.0)	64.29 (2.92)	305.24 (21.23)	495.40 (17.47)	0.056 (0.005)
	2	31.36 (4.21)	84.41 (5.21)	0.200 (0.049)	31.36 (4.21)	0.000 (0.0)	53.06 (8.26)	227.57 (99.26)	463.86 (9.81)	0.073 (0.041)
	3	28.82 (5.46)	74.86 (5.85)	0.172 (0.045)	28.82 (5.46)	0.000 (0.0)	46.04 (7.68)	272.12 (122.13)	470.53 (20.61)	0.061 (0.040)
	4	35.91 (1.25)	85.82 (2.96)	0.189 (0.013)	35.91 (1.25)	0.000 (0.0)	49.91 (2.57)	293.46 (21.76)	409.91 (29.41)	0.052 (0.008)
9	1	36.80 (4.74)	89.46 (8.99)	0.207 (0.015)	14.87 (2.60)	0.704 (0.040)	52.66 (5.64)	269.96 (22.26)	451.87 (25.44)	0.058 (0.005)
	2	28.40 (1.81)	61.47 (3.11)	0.116 (0.010)	17.98 (0.95)	0.740 (0.124)	33.06 (3.07)	265.99 (29.25)	400.62 (12.20)	0.047 (0.007)
	3	35.29 (5.08)	70.12 (6.50)	0.113 (0.015)	19.42 (2.52)	0.722 (0.113)	34.84 (4.72)	398.01 (48.28)	505.49 (26.52)	0.026 (0.009)
	4	35.00 (2.05)	74.88 (1.89)	0.142 (0.010)	17.39 (2.37)	0.720 (0.147)	39.88 (1.59)	303.63 (13.97)	399.41 (24.07)	0.045 (0.003)

Table 11. (Continued).

Subj	Cond	Cont	Max	Tmax	Min	Tmin	ROM	ContVel	MaxVel	TmaxVel
10	1	37.30 (4.75)	106.88 (6.61)	0.290 (0.083)	29.83 (7.69)	0.495 (0.452)	69.57 (7.17)	413.64 (39.35)	512.40 (33.66)	0.046 (0.012)
	2	22.59 (2.43)	62.32 (6.38)	0.135 (0.005)	18.59 (1.93)	0.660 (0.369)	39.73 (4.49)	293.79 (56.69)	409.39 (50.83)	0.050 (0.011)
	3	33.32 (7.49)	76.92 (9.46)	0.142 (0.012)	18.87 (5.21)	0.650 (0.364)	43.59 (5.54)	412.79 (62.41)	525.73 (37.25)	0.031 (0.010)
	4	31.66 (3.64)	81.84 (9.25)	0.166 (0.023)	29.54 (5.86)	0.165 (0.369)	50.19 (6.71)	359.77 (18.09)	463.50 (39.06)	0.043 (0.012)

Note: Angle and ROM units are in degrees and time unit is in seconds.

Velocity unit is in deg/s.

Standard deviation values are in parenthesis.

The definitions of variables are in Appendix H

APPENDIX T

SUBJECT ANGULAR KINEMATIC ANKLE JOINT DATA

Table 12 . Subject means and standard deviations of angular kinematic ankle joint variables.

Subj	Cond	Cont	Max	Tmax	Min	Tmin	ROM	Cont Vel	Max Vel	Tmax Vel
1	1	-13.24 (2.83)	29.90 (0.62)	0.148 (0.016)	-13.24 (2.83)	0.000 (0.0)	43.14 (2.34)	459.81 (79.75)	553.95 (43.14)	0.025 (0.008)
	2	-11.88 (4.10)	28.85 (1.0)	0.164 (0.025)	-11.88 (4.10)	0.000 (0.0)	40.73 (3.57)	400.43 (58.93)	493.40 (38.08)	0.025 (0.006)
	3	-14.01 (3.69)	29.54 (3.23)	0.136 (0.010)	-14.01 (3.69)	0.000 (0.0)	43.55 (5.71)	364.35 (84.08)	534.09 (43.92)	0.033 (0.010)
	4	-18.53 (2.17)	24.59 (1.71)	0.124 (0.004)	-18.53 (2.17)	0.000 (0.0)	43.12 (2.43)	429.48 (23.90)	556.92 (29.39)	0.030 (0.002)
2	1	-4.25 (2.55)	30.49 (0.92)	0.186 (0.074)	-4.25 (2.55)	0.000 (0.0)	34.74 (2.23)	315.76 (44.30)	406.19 (12.49)	0.028 (0.008)
	2	-7.84 (3.63)	27.49 (2.28)	0.147 (0.017)	-7.84 (3.63)	0.000 (0.0)	35.33 (4.58)	347.02 (48.30)	431.17 (38.39)	0.026 (0.005)
	3	0.25 (3.64)	31.83 (1.79)	0.144 (0.023)	0.25 (3.64)	0.000 (0.0)	31.58 (4.32)	368.47 (71.38)	417.27 (63.76)	0.020 (0.006)
	4	-18.50 (0.79)	25.38 (0.40)	0.128 (0.008)	-18.50 (0.79)	0.000 (0.0)	43.88 (1.04)	467.80 (49.89)	561.49 (36.06)	0.027 (0.004)
3	1	-18.36 (0.62)	29.66 (1.10)	0.174 (0.028)	-18.36 (0.62)	0.000 (0.0)	48.02 (1.31)	468.11 (40.39)	585.20 (25.61)	0.028 (0.003)
	2	-20.99 (1.93)	24.38 (2.47)	0.124 (0.009)	-20.99 (1.93)	0.000 (0.0)	45.37 (3.05)	466.88 (39.32)	581.49 (29.19)	0.027 (0.005)
	3	14.56 (4.02)	20.76 (2.47)	0.069 (0.024)	4.98 (7.04)	0.587 (0.291)	6.20 (5.90)	109.03 (102.80)	127.93 (102.76)	0.177 (0.362)
	4	-26.80 (1.77)	12.26 (3.91)	0.473 (0.330)	-26.80 (1.77)	0.000 (0.0)	39.06 (5.16)	421.48 (40.62)	517.00 (73.28)	0.025 (0.003)

Table 12. (Continued).

Subj	Cond						Cont	Max	Tmax	
		Cont	Max	Tmax	Min	Tmin	ROM	Vel	Vel	Vel
4	1	-22.38 (7.23)	27.93 (17.02)	0.320 (0.288)	-22.72 (7.16)	0.130 (0.291)	50.31 (16.87)	363.01 (93.98)	588.67 (96.81)	0.174 (0.313)
	2	-22.48 (4.95)	19.05 (3.35)	0.137 (0.036)	-22.48 (4.95)	0.000 (0.0)	41.53 (3.91)	393.36 (45.91)	550.30 (126.43)	0.030 (0.003)
	3	-1.46 (4.48)	19.76 (2.89)	0.133 (0.019)	-1.46 (4.48)	0.000 (0.0)	21.22 (6.96)	213.42 (46.59)	284.30 (52.32)	0.025 (0.014)
	4	-21.79 (4.58)	18.21 (8.38)	0.111 (0.025)	-21.79 (4.58)	0.000 (0.0)	40.00 (11.56)	437.11 (128.48)	577.24 (113.25)	0.027 (0.016)
5	1	-17.45 (4.19)	39.55 (3.24)	0.245 (0.035)	-17.45 (4.19)	0.000 (0.0)	57.00 (3.78)	433.24 (78.84)	576.87 (28.02)	0.032 (0.010)
	2	-20.41 (2.64)	18.69 (3.28)	0.110 (0.009)	-20.41 (2.64)	0.000 (0.0)	39.10 (3.42)	454.73 (47.23)	561.25 (41.18)	0.026 (0.004)
	3	-16.74 (3.96)	18.85 (3.89)	0.111 (0.008)	-16.74 (3.96)	0.000 (0.0)	35.59 (3.48)	394.66 (43.11)	504.10 (38.19)	0.027 (0.004)
	4	-21.14 (3.81)	18.53 (2.17)	0.087 (0.007)	-33.35 (2.49)	0.312 (0.012)	39.67 (4.60)	622.72 (29.92)	705.83 (36.59)	0.018 (0.004)
6	1	4.38 (8.68)	34.06 (1.95)	0.134 (0.015)	1.98 (4.45)	0.330 (0.452)	29.68 (8.32)	428.78 (70.72)	460.11 (70.68)	0.012 (0.013)
	2	2.87 (4.76)	32.27 (3.39)	0.145 (0.014)	2.87 (4.76)	0.000 (0.0)	29.40 (6.97)	328.62 (94.18)	376.28 (109.36)	0.020 (0.003)
	3	20.93 (1.48)	27.65 (3.29)	0.112 (0.013)	13.17 (2.39)	0.808 (0.023)	6.71 (2.59)	71.07 (44.39)	93.88 (43.12)	0.033 (0.020)
	4	-14.11 (1.31)	20.15 (4.92)	0.114 (0.007)	-14.11 (1.31)	0.000 (0.0)	34.26 (4.04)	362.72 (21.87)	467.87 (39.85)	0.028 (0.003)

Table 12 . (Continued).

Subj	Cond	Cont	Max	Tmax	Min	Tmin	ROM	Cont Vel	Max Vel	Tmax Vel	
7	1	-5.12	32.42	0.186	-5.12	0.000	37.55	386.25	451.23	0.023	
		(1.73)	(2.18)	(0.038)	(1.73)	(0.0)	(1.72)	(19.99)	(14.86)	(0.002)	
	2	-4.25	25.37	0.115	-4.25	0.000	29.63	390.80	448.41	0.019	
		(3.89)	(2.02)	(0.017)	(3.89)	(0.0)	(5.24)	(64.70)	(24.30)	(0.012)	
	3	7.72	20.36	0.079	1.89	0.293	12.64	199.49	226.31	0.102	
		(4.75)	(3.22)	(0.046)	(5.91)	(0.176)	(7.27)	(141.96)	(129.25)	(0.195)	
	4	-12.82	27.21	0.287	-12.82	0.000	40.04	426.52	501.11	0.023	
		(3.95)	(2.13)	(0.205)	(3.95)	(0.0)	(5.17)	(59.02)	(44.10)	(0.005)	
	8	1	-11.21	26.87	0.292	-11.21	0.000	38.08	394.38	462.74	0.023
			(5.76)	(2.48)	(0.164)	(5.76)	(0.0)	(5.49)	(57.78)	(69.44)	(0.002)
		2	-17.20	24.08	0.201	-17.20	0.000	41.28	295.58	471.46	0.042
			(11.80)	(1.56)	(0.057)	(11.80)	(0.0)	(12.49)	(141.91)	(90.80)	(0.035)
3		-8.71	21.13	0.172	-8.75	0.004	29.85	234.70	364.97	0.039	
		(3.07)	(1.38)	(0.046)	(3.13)	(0.009)	(4.23)	(140.20)	(33.52)	(0.036)	
4		-22.31	14.56	0.259	-22.31	0.000	36.87	353.13	462.90	0.031	
		(3.69)	(6.25)	(0.307)	(3.69)	(0.0)	(3.64)	(86.19)	(63.03)	(0.007)	
9		1	-10.36	29.05	0.164	-10.36	0.000	39.41	369.26	471.84	0.030
			(1.79)	(1.36)	(0.042)	(1.79)	(0.0)	(2.88)	(44.37)	(17.22)	(0.008)
		2	-15.64	21.99	0.115	-15.64	0.000	37.62	410.13	513.72	0.027
			(1.85)	(3.52)	(0.007)	(1.85)	(0.0)	(3.96)	(31.58)	(31.88)	(0.005)
	3	8.71	24.54	0.112	2.90	0.483	15.83	191.11	232.47	0.018	
		(10.77)	(4.67)	(0.024)	(6.88)	(0.298)	(8.73)	(81.48)	(113.14)	(0.007)	
	4	-22.09	8.89	0.208	-23.36	0.092	30.98	344.65	414.32	0.027	
		(2.03)	(2.18)	(0.212)	(4.0)	(0.205)	(4.18)	(32.07)	(52.28)	(0.004)	

Table 12. (Continued).

Subj	Cond	Cont	Max	Tmax	Min	Tmin	ROM	Cont Vel	Max Vel	Tmax Vel
10	1	-21.70 (1.90)	19.36 (1.56)	0.218 (0.120)	-21.70 (1.90)	0.000 (0.0)	41.06 (2.79)	428.31 (73.92)	509.11 (49.63)	0.028 (0.008)
	2	-25.41 (1.93)	13.05 (1.29)	0.178 (0.085)	-25.41 (1.93)	0.000 (0.0)	38.46 (1.49)	442.31 (33.91)	510.28 (20.50)	0.023 (0.002)
	3	-0.77 (12.57)	23.69 (1.26)	0.134 (0.007)	-4.25 (8.89)	0.165 (0.369)	24.45 (13.61)	239.32 (121.13)	314.03 (164.92)	0.023 (0.011)
	4	-28.05 (6.20)	6.93 (5.79)	0.114 (0.017)	-28.05 (6.20)	0.000 (0.0)	34.97 (3.73)	477.66 (86.97)	527.75 (61.73)	0.018 (0.008)

Note: Angle and ROM units are in degrees and time unit is in seconds.

Velocity unit is in deg/s.

Standard deviation values are in parenthesis.

The definitions of variables are in Appendix H.

Vita

Kurt Gavin Clowers was born in Lynchburg, Virginia, January 15, 1974. His family moved to Roanoke, Virginia when Kurt was a small child. He attended Cave Spring High School from 1989-92 and continued his education at Virginia Tech where he received his first bachelor's degree in biology in 1996. From there, he attended The University of Tennessee and obtained his second bachelor's degree in exercise science and became a lifetime member of the Golden Key Honor Society. In the fall of 2002 he completed his master's degree in human performance and sport studies/biomechanics education at The University of Tennessee and graduated Summa Cum Laude.

Kurt married his wife Cheryl in October 2002 and he began his next goal, to seek a Ph.D. in biomechanics at The University of Tennessee. He anticipates obtaining his degree by the end of the spring semester 2005.